

# Dimensioning current cycles for High Voltage Components in Battery Electric Vehicles

Analysis and evaluation of High Voltage Cables in Battery Electric Vehicle for different driving cycles

Master's thesis in Electric Power Engineering

Prarthana Ramesh Jayaraman  
Sathiyam Srinivasan



MASTER'S THESIS 2019

# Dimensioning current cycles for High Voltage Components in Battery Electric Vehicles

Analysis and evaluation of High Voltage Cables in Battery Electric  
Vehicle for different driving cycles

Prarthana Ramesh Jayaraman  
Sathiyar Srinivasan



**CHALMERS**  
UNIVERSITY OF TECHNOLOGY

Department of Electrical Engineering  
*Division of Electric Power Engineering*  
CHALMERS UNIVERSITY OF TECHNOLOGY  
Gothenburg, Sweden 2019

Dimensioning current cycles for High voltage components in Battery Electric Vehicles  
Analysis and evaluation of High Voltage Cables in Battery Electric Vehicle for different drive cycles

Prarthana Ramesh Jayaraman  
Sathiyam Srinivasan

© Prarthana Ramesh Jayaraman & Sathiyam Srinivasan, 2019.

Supervisor: Anders Lasson , (97150) EPS CAE System Design, Volvo Car Corporation  
Examiner: Torbjörn Thiringer, Electric Power Engineering, Chalmers University of Technology

Master's Thesis 2019  
Department of Electrical Engineering  
Division of Electric Power Engineering  
Chalmers University of Technology  
SE-412 96 Gothenburg  
Telephone +46 31 772 1000

Cover: Flow diagram for the selection of customer based on usage  
Printed by Chalmers Reproservice  
Typeset in L<sup>A</sup>T<sub>E</sub>X  
Gothenburg, Sweden 2019

# Dimensioning current cycles for High Voltage components in Battery Electric Vehicles

Prarthana Ramesh Jayaraman

Sathiyam Srinivasan

Department of Electrical Engineering

Division of Electric Power Engineering

Chalmers University of Technology

## Abstract

In this thesis, an algorithm is proposed to determine the current cycles for high voltage cables in BEVs based on customer usage. In order to determine the lifetime of the cables, a thermal lumped parameter model is implemented that could determine the transient response of the cable temperature from the drive cycles. The fitting of thermal parameters as a function of the cable temperature and geometry is investigated. An Arrhenius ageing model is proposed to calculate the useful life of the cable for cable temperatures and different cable classes. Additionally, the damage value of the cable is calculated from Miner's rule in terms of loss-of-life fractions. For this evaluation, the current cycles are obtained from an existing vehicle simulation model for different drive cycles. A set of driver types are created to understand the customer usage patterns, depending on their driving behaviour and their share in each drive cycle. These driver types are further used to generate a customer population based on the frequency of occurrence of each driver type. This thesis further proposes a statistical approach to select the cable based on the 90<sup>th</sup> percentile customer usage and further determine their current cycles based on the customer's driving share in each drive cycle.

It was found that, the damage value of the cable was 0.733 for a cable belonging to class 3, while a damage value of  $2.06 \cdot 10^{-2}$  was observed for a class 4 cable in the case of the 90<sup>th</sup> percentile customer investigated (A damage value of 1 means the end of life for the cable), i.e., when using a 50 mm<sup>2</sup> cable for a reference composed drive cycles and a total mileage of 350000 km. Additionally, by using the probability distribution function, it was observed that the 90<sup>th</sup> percentile customer belonged to the driver type with the highest autobahn driving share in all cases, irrespective of the cable class used. Furthermore, the usage of cables at an ambient temperature of 65°C resulted in a damage value that was 10<sup>5</sup> times greater than the cables utilised at an ambient temperature of 20°C. Finally, worth mentioning is that the addition of a 50 kW fast charger to the combined drive cycles had a minimal influence on the cable life.

Keywords: high voltage cables, current cycles, customer usage, vehicle simulations, lumped parameter model, Arrhenius ageing model, Miner's rule, customer population, 90<sup>th</sup> percentile customer, fast charging.



# Acknowledgements

We are grateful to Volvo Cars Corporation for providing us with the infrastructure and resources towards the execution of this thesis work.

Firstly, we immensely appreciate our supervisor, Anders Lasson, for his tremendous support and continuous commitment to the successful completion of this thesis work. We would also like to thank our Manager, Peter Berggren, for trusting us and providing us with the opportunity to be a part of this project and welcoming us very warmly in the team. It was a fantastic opportunity to work with the team, EPS CAE System Design and receive timely support from the team members. Thank you for encouraging us and being patient with us throughout our work.

We would like to extensively thank Jan Andersson and Michael Svensson from the Transmission Department at VCC, for their continuous support and their insights regarding the methodology proposed in this thesis.

A special thanks to Sriram Mandayam for his insights regarding the thermal behaviour of the components and David Martin Gonzalez for his support by providing the supplier's information for the components and understanding the electrical aspects of each component.

We want to offer special gratitude and thanks to our examiner, Torbjörn Thiringer for his continuous support and advice at every stage in the thesis work and also motivating us to achieve the goals of this thesis.

Finally, we would like to thank our family and friends for all support and encouragement throughout the project and also our study in Chalmers.

Prarthana Ramesh Jayaraman  
Sathiyam Srinivasan, Gothenburg, October 2019



# Contents

<b>1</b>	<b>Introduction</b>	<b>1</b>
1.1	Background . . . . .	1
1.2	Previous work . . . . .	1
1.3	Purpose of work . . . . .	2
1.4	Scope . . . . .	2
<b>2</b>	<b>BEV powertrain and system description</b>	<b>3</b>
2.1	High Voltage Distribution System . . . . .	4
2.1.1	Generation of fast charging current cycle . . . . .	5
2.2	High Voltage Distribution System Components for BEVs . . . . .	6
2.2.1	Fuse . . . . .	6
2.2.2	Contactors . . . . .	7
2.2.3	HV Connectors . . . . .	7
2.2.4	High Voltage Cables . . . . .	8
<b>3</b>	<b>Theory</b>	<b>9</b>
3.1	Cable Thermal Model . . . . .	9
3.1.1	Heat transfer mechanism within cables . . . . .	9
3.1.1.1	Conduction . . . . .	9
3.1.1.2	Convection . . . . .	10
3.1.1.3	Thermal Power loss in cables . . . . .	10
3.1.2	Elements of LPN model . . . . .	12
3.1.3	Fitting of thermal parameters to the data sheet . . . . .	15
3.2	Ageing of Cables . . . . .	15
3.2.1	Arrhenius ageing model . . . . .	16
3.2.1.1	Determination of Arrhenius Constants . . . . .	16
3.2.2	Damage Value . . . . .	17
<b>4</b>	<b>Method set-up</b>	<b>19</b>
4.1	Overview of key procedures . . . . .	20
4.2	Vehicle Simulations . . . . .	20
4.3	Cable Thermal model simulation . . . . .	21
4.4	Procedure for life and damage value calculation . . . . .	23
4.5	Generation of customers/drivers . . . . .	24
4.5.1	Basic drive cycles . . . . .	24
4.5.1.1	Distance-based drive cycles . . . . .	24

4.5.1.2	Event-based drive cycles . . . . .	26
4.5.1.3	Simulated current for different drive cycles . . . . .	28
4.5.2	Share of drive cycles for different driver types . . . . .	29
4.5.3	Aggressiveness share for different driver types . . . . .	30
4.5.4	Percentage share of total drivers . . . . .	32
4.5.4.1	Behaviour distribution in the customer population . . . . .	33
4.6	Statistical method for selecting 90 <sup>th</sup> percentile customer . . . . .	33
4.7	Matlab script process flow . . . . .	36
<b>5</b>	<b>Base Verification</b>	<b>39</b>
5.1	Sensitivity of parameters with change in temperature . . . . .	39
5.1.1	Variation of thermal conductivity with conductor temperature . . . . .	39
5.1.2	Variation of thermal resistance with conductor temperature . . . . .	40
5.1.3	Temperature model for steady-state current . . . . .	42
5.1.4	Time to reach steady-state . . . . .	44
5.1.5	Influence of heat transfer coefficient on conductor temperature . . . . .	45
5.1.6	Impact of change in conductor geometry on cable temperature . . . . .	46
<b>6</b>	<b>Analysis</b>	<b>47</b>
6.1	Cable thermal analysis for different drive cycles . . . . .	47
6.1.1	Temperature determination for distance-based cycles . . . . .	47
6.1.2	Temperature determination for event-based cycles . . . . .	49
6.1.3	Arrhenius ageing model for drive cycles . . . . .	50
6.1.3.1	Arrhenius parameters . . . . .	50
6.1.4	Impact of aggressiveness on damage value for basic drive cycles . . . . .	51
6.1.5	Damage value spectra for customer population . . . . .	52
6.1.5.1	Selection of cable class . . . . .	53
6.1.5.2	Selection of 90 <sup>th</sup> percentile customer . . . . .	54
6.2	Creating current cycles for 90 <sup>th</sup> percentile customer . . . . .	55
6.3	Influence of ambient temperature on the cable usage . . . . .	57
6.4	Influence of convective cooling on the cable usage . . . . .	58
6.5	Impact of mileage accumulation and fast charging on cable ageing . . . . .	59
6.5.1	Impact of combined drive cycles on cable conductor temperature . . . . .	60
6.5.2	Damage value analysis for combined drive cycles . . . . .	63
6.5.3	Influence of different charging rates on cable life . . . . .	64
<b>7</b>	<b>Conclusion</b>	<b>65</b>
7.1	Future work . . . . .	65
	<b>Bibliography</b>	<b>67</b>
<b>A</b>	<b>Appendix 1</b>	<b>I</b>
A.1	Cable conductor temperature plot from the data sheet . . . . .	II
A.2	Cable parameters . . . . .	III
A.2.1	Geometrical parameters . . . . .	III
A.2.2	Calculation of conductor temperature for steady state condition (50mm <sup>2</sup> ) . . . . .	III

A.2.3	MATLAB code for calculation of cable conductor temperature	IV
A.2.3.1	Input parameters code and save file name as:cable . .	IV
A.2.3.2	Execution code or Run code and and save file name as:cable1 . . . . .	V



# 1

## Introduction

### 1.1 Background

The developing trends in the automotive industry are to overcome the challenges of reducing the  $CO_2$  emissions and dependence on fossil fuels. The vehicle manufacturers embraced the concept of electrified powertrains to comply with the strict regulations set by the European Commission, according to [9]. In this light, battery electric vehicles (BEVs) have a higher powertrain efficiency and produce zero emissions when compared to the conventional vehicles [30]. Today's OEMs have their electric vehicle model, yet the BEVs are not commercially manufactured on a large-scale, world-wide[30]. The drawbacks of relatively short-range, long charging time and cost constraints need to be addressed for the BEVs to compete with the conventional vehicles in the market.

In BEVs, the DC currents in the High Voltage (HV) system have large fluctuations. With the primary focus of reducing costs and weight, the system design has to overcome the current overloads to the HV components. It is essential to understand the dynamic response of these components based on customer usage. The wear of the HV components are non-linear and therefore overloading of these components induce ageing/fatigue. The ageing causes premature failures such as fuse melting, cable damage, contactor wear, connector damage, etc. In order to select these components, the use-cases (i.e. DC cycles and how the continuous usage affects the component during the vehicle's life) have to be defined.

### 1.2 Previous work

The transmission department at VCC was required to develop new concepts to accurately predict loads on the transmission components with simulations and vehicle measurements. It requires representative assumptions of real-world customer usage data. The drive cycles were retrieved using the diagnostic readout (DRO) data, which is logged in cars and extracted later [29].

Utilising a synthetic customer population, the transmission department developed a model-based algorithm for transmission components [29], specifically for the gear mechanism, based on customer usage. The main parameters in their study included torque and the number of revolutions. A calculation script was developed based on these parameters to calculate the lifetime of the components and damage value for

each customer based on the usage of drive cycles. A probability distribution curve for each customer with their respective damage values based on the drive cycles was created to analyse the usage pattern of the 90<sup>th</sup> percentile customer.

### 1.3 Purpose of work

The primary purpose of the thesis is to determine the current cycles for HV components in BEVs based on customer usage. A cable thermal model is to be developed to investigate the dynamic behaviour of the conductor temperature. Moreover, an algorithm-based calculation script is to be developed to predict the lifetime of the cables, taking into account the driving behaviour in different drive cycles. Finally, the methodology to select the 90<sup>th</sup> percentile customer is investigated to determine the current cycles and select the most suitable cable class based on the defined usage.

### 1.4 Scope

The goal of the thesis work is to develop a methodology to determine the use-cases (i.e. DC-current cycles and how many times they occur during the vehicle's life). The method shall be based on the vehicles usage (drive cycles) and the HV components damage mechanisms.

- The vehicle simulation to calculate the current cycles are performed in an existing vehicle simulation package. This model does not need to be developed.
- A life estimation model is to be developed to calculate the useful life of the cable, and thereby calculate the damage occurred due to the usage in the different drive cycles.
- The method to generate customer population uses previous knowledge from the Transmission department at VCC and further develop the model based on some of the assumptions for HV components.
- During this work, a complete Matlab script is to be developed to find and analyse the usage pattern of the 90<sup>th</sup> percentile driver.
- The influence of combined drive cycles and fast charging on the cable life is to be investigated.

# 2

## BEV powertrain and system description

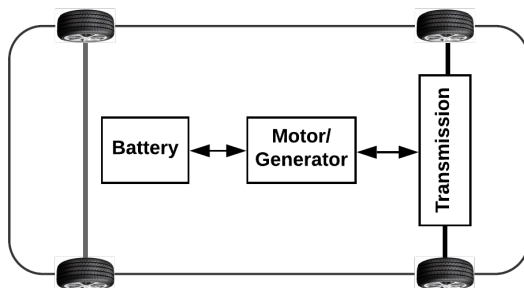


**Figure 2.1:** Simple sketch of a BEV powertrain

A battery electric vehicle (BEV) consists of an electric drive system which is powered by a battery pack and one or more electric motors. A basic BEV powertrain model is depicted in Figure 2.1. The BEV powertrain also consists of one or several transmission systems connected to the wheel shaft(s) via a gearbox(es) and a differential(s). The electrical energy from the battery is transferred to the motor through a DC/AC power converter, which controls the frequency and voltage magnitude. The selection of appropriate cables for various positions in the vehicle is an important issue. The electrical energy transfer depends on the driver's interaction with the acceleration and/or braking pedal, vehicle type, and external factors that act on the vehicle while driving, such as air drag, rolling resistance and grading (during the slope). The electric machine can operate in both motoring and generation modes during the propulsion of the vehicle. During braking, the electric machine operates in generation mode as a conventional alternator, by converting the mechanical to electrical energy and thus recharging the battery. While operating in motoring mode, a high torque output requires a high current input, and high speed requires an increased voltage input. Due to the time-varying actions and load demand, the HV components are loaded in different patterns.

## 2.1 High Voltage Distribution System

A simplified electric diagram of the HV system is presented in Figure 2.2 below.

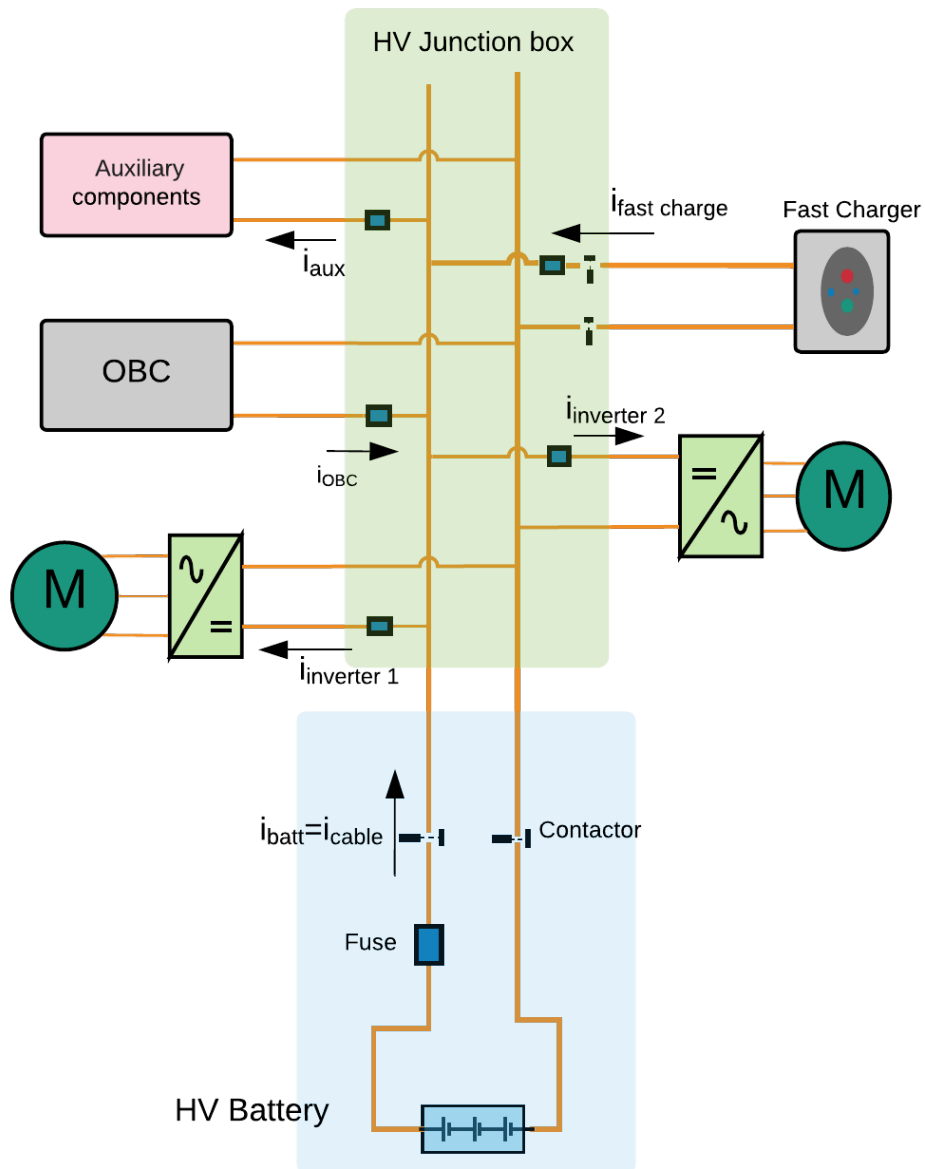


**Figure 2.2:** HV distribution system and its components in BEVs

The HV distribution system shown in the figure above is the type of system used for electrical system studies in this thesis. The electrical system comprises an energy storage system, two electric motor drive systems, and auxiliary HV components. The power in the electrical system is transmitted through the HV distribution network which includes fuses, contactors, cables, and connectors to the load.

The HV system is designed in such a way that it satisfies the different consumer usages and protects the system against possible overloads and short circuits. It ensures the protection from over currents, overheating and arcs during accidents, and thus protects the electrical distribution system from getting damaged and the customer from electric shocks.

According to Figure 2.2, the battery current  $i_{batt}$  is considered to be equal to the current carried by the cable  $i_{cable}$ . Thus the cable current is the summation of current to the inverters and current supplied to the other auxiliary loads. The battery current  $i_{batt}$  and cable current  $i_{cable}$  can be written according to Figure 2.2 as

$$i_{cable} = i_{batt} = i_{inverter1} + i_{inverter2} + i_{aux} \quad (2.1)$$

During fast charging, the rest of the system is isolated, and the battery current equals the fast charging cable current and can be written as

$$i_{cable} = i_{fastcharge} \quad (2.2)$$

### 2.1.1 Generation of fast charging current cycle

Figure 2.3 shows two consecutive charging phases of the Li-ion battery, according to [18].

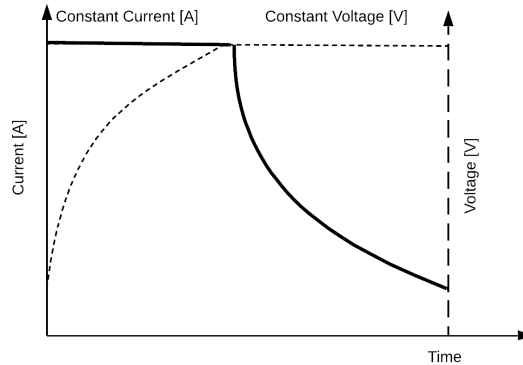


**Figure 2.3:** Typical fast charging profile of Li-ion battery

It is observed from Figure 2.3 that the first phase is initiated when the driver puts in the cable to the socket and the battery can be at 10%, 30%, 50%, 70% SOC. This phase is referred to as the constant current (CC) phase. In the CC mode, the voltage is increased gradually, and the current is kept constant until the voltage reaches its limit. During the second phase, the voltage is kept constant, and the current will

decline approximately towards the minimum limit set by the battery management system. It is called a constant voltage (CV) phase.

## 2.2 High Voltage Distribution System Components for BEVs

As discussed in Section 2.1, the HV distribution system components are fuses, cables, contactors, and connectors. This section addresses the underlying principles of the HV distribution system components. The prime focus of this work is the HV cables, but since the components such as connectors, contactors, fuses, and cables are connected in the system, and are selected based on each of the preceding component ratings, the other components are also discussed.

### 2.2.1 Fuse

A fuse is a protection device used in an electrical circuit to protect the circuit if an overcurrent occurs. It has a fusible link consisting of a metal wire or a strip which melts when a high current flows through the fuse, and it permanently breaks the circuit. The fuses and cables are chosen such that the fuse protects the cables at faults (short-circuits) without causing damage to the cables by the current loads. Hence, appropriate fuse selection is highly important. Figure 2.4 presents a typical parameter for a fuse operating in a circuit, a fuse takes a certain amount of time before they open under a critical condition called ‘reaction time’ (pre-arcing time + arcing time).

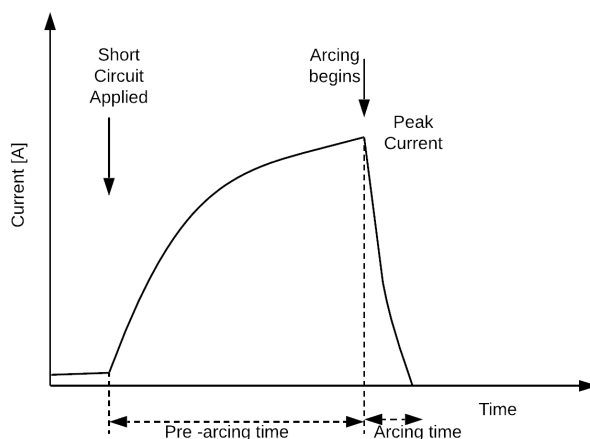


**Figure 2.4:** Fuse arcing characteristic

The time before the internal wire in the fuse melts, thermal energy is generated from the current this is known as the melting integral of a fuse or termed as  $I^2t$ . The melting  $I^2t$  of the fuse is one of the values which is used in the selection and sizing of a fuse, where  $I$  is the current and  $t$  is the time for the fuse to melt [15].

Figure 2.5 shows that if the fuse is exposed to a consistent current pulses, the lifetime of the fuse can be determined by the  $I^2t$  characteristics curve comprising of the rated capacity and the number of cycles.

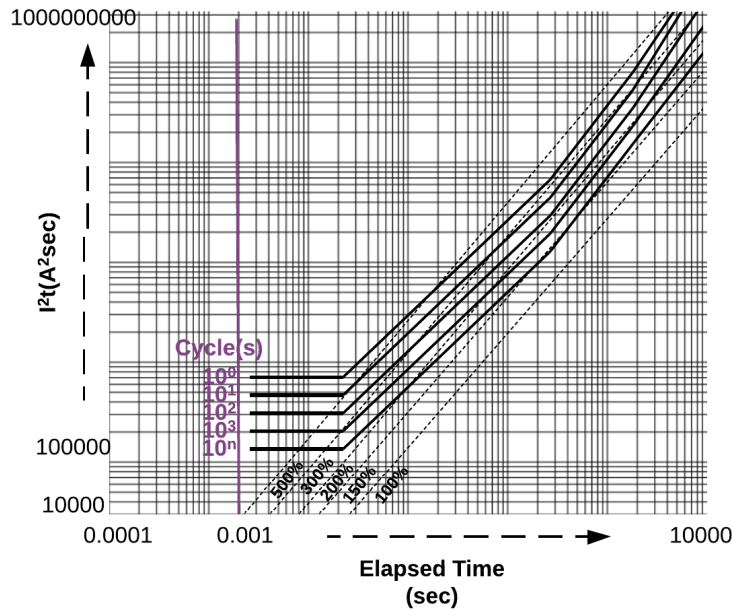


**Figure 2.5:** Typical HV fuse  $I^2t$  Characteristic curve

The durability or the service life of the fuse depends on the load, current waveforms, ambient temperatures, and other factors. The rated capacity represents the ability of the fuse element to melt within the maximum opening time at designated overload points (typically 100% to 500% of the fuse rating).

## 2.2.2 Contactors

A contactor is an electromechanical switching device, which uses a coil to generate a magnetic force that mechanically operates an electrical contact. The technical need for the contactors is to switch the live components during the possible needed situations. The contactors connect and break the circuits, sometimes under the maximum load conditions. The breaking capacities of load contactors are determined by the product of current-voltage during the load breaking and could be several 100 kW, according to [5].

## 2.2.3 HV Connectors

The selection of HV power connectors for the components in the vehicle is of high importance. The connectors connect the cables to the electric machines, power electronic components, battery, which has to withstand vibrations from the road, from the combustion engine (in case of hybrid), and motor, then the high-temperature changes due to variations in current, humidity, and a corrosive environment [12].

So, the connectors have to withstand different stresses during the entire life of the vehicle.

### 2.2.4 High Voltage Cables

There are several analytical and numerical approaches available for defining the current rating of electrical cables at steady-state operations, the analytical approaches are based on the IEC 60287 standard [31], and they can only be applied in homogeneous ambient conditions and on simple geometries. And the standards are not application specific for automotive usage.

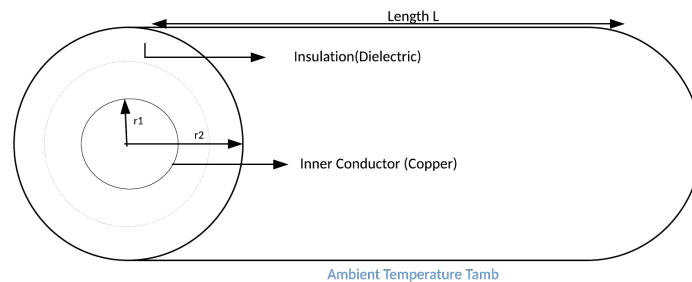


**Figure 2.6:** Cylindrical cable with inner conductor and insulation

The current carrying capacity of cable shown in Figure 2.6 implies the maximum current value that the cable conductor can transmit continuously without overshooting the temperature limit of the cable for different cable classes, in particular not exceeding that of the insulating material. Thus, the temperature values of the cable components throughout continuous operation should be determined. Numerical methods are applied for the calculation of temperature distribution in a cable and its surrounding environment, based on the heat generated inside the cable. For this purpose, the conductor temperature is determined for a presented conductor current based on the load conditions, and the calculations are scripted using ambient temperature conditions, geometry, and material information. In this study, the variation of thermal conductivity with the temperature is considered, and further, the loss and heating mechanisms were evaluated together.

# 3

## Theory

This chapter presents a thermal circuit model that is used for the prediction of the dynamic response of the cable conductor temperature due to varying current loads and ambient air. In case of an overload condition, the transient temperature behaviour reduces the lifetime of the cables. So, to understand the usage of the cables in different drive cycles, an ageing model is proposed to calculate the remaining life and further to estimate the damage created to the cables.

### 3.1 Cable Thermal Model

The study of the thermal behaviour of the cable is an important segment in the system design. The efficient dissipation of inherent cable losses determines the maximum current carrying capacity of the cables [22]. At full load operations, the conductor temperature reaches within the selected cable class operating temperature range. Whereas, in the case of an overload condition, the conductor temperature rises excessively for a short time [22]. This could result in damage to the cable material properties, thus accelerating the process of the cables reaching its useful life. The conductor temperature is determined according to the temperature at the outer surface of the cable [22]. Additionally, to calculate the damage to the cable insulation, it is necessary to understand why heat is generated within the cables, how heat is distributed to the cable surface and the temperature difference between the cable surface and the ambient air [22]. Based on the heat transfer principles, an equivalent thermal circuit for a single-core cable is proposed to calculate the transient response of the cable core temperature to the changes in the current load.

#### 3.1.1 Heat transfer mechanism within cables

The heat is generated in the conductor and is transferred to the ambient via the cable insulation. Generally, heat is transferred from an elevated temperature region to the lower temperature region [11]. This heating phenomenon is attributed to as Joule or Ohmic heating [14]. According to the principles of heat transfer, there are three mechanisms of heat transfer: conduction, convection and radiation [11].

##### 3.1.1.1 Conduction

According to Fourier's law, the heat transfer by conduction can be described as heat flux over material is proportional to the negative gradient of temperature and the

area. The heat flow is perpendicular to that temperature gradient. Therefore, the heat conduction is characterised by the rate equation for cylindrical coordinates in the radial direction only [11, 25], according to

$$Q = -k_{ins}A_c \frac{dT}{dr} \quad (3.1)$$

where  $Q$  is the heat flux in  $[W/m^{-2}]$ ,  $T$  is the temperature at the outer surface of the cable conductor in  $[K]$ , and radius  $r$  in radial position  $[m]$ ,  $A_c$  is the conductor surface area in  $[m^2]$  and  $k_{ins}$  is the thermal conductivity of the insulation material in  $[W/m \cdot K]$ . The thermal conductivity  $k_{ins}$  is a physical property of material which is a measure of its ability to conduct heat [13]. The negative sign in (3.1) indicates that heat always flows in the direction of decreasing temperature.

#### 3.1.1.2 Convection

Convection is defined as the heat transfer from one medium to another by the movement of a fluid (water or air) either by natural or forced cooling. The convective heat transfer is also referred to as the Newton's Law of Cooling and is represented as

$$Q = hA_c(T_c - T_{amb}) \quad (3.2)$$

where  $Q$  is the heat flux in  $[W/m^{-2}]$ ,  $h$  is the convective heat transfer  $[W/m^2 \cdot K]$ ,  $T_c$  is the cable surface temperature and  $T_{amb}$  is the ambient temperature from the outer surface in  $[K]$ .

#### 3.1.1.3 Thermal Power loss in cables

The heat generated within the cable is transferred through the insulation medium into the surroundings by the conduction mechanism, as seen in (3.1). During heat transfer, power loss occurs in the conductor [13, 31] and is given according to

$$P_{elec,loss} = i_{cable}^2 R_c \quad (3.3)$$

where  $P_{elec,loss}$  is the conductor loss,  $R_c$  is the electrical cable resistance. The electrical resistance of the conductor  $R_c$  is dependant on the cross-sectional area as well as it's material properties [13, 31] and is given according to

$$R_c = \rho \frac{L}{A_c} \quad (3.4)$$

where  $\rho$  is the electrical resistivity of the conductor material,  $L$  is the length of the cable and  $A_c$  is the cross-sectional area of the conductor. The resistivity is an intrinsic property of the conductor material, offering resistance to the mobility of the electrons. The conductor resistance per unit metre, as a function of temperature [31] can be written according to

$$R_c = R_0[1 + \alpha(T_c - T_0)] \quad (3.5)$$

where  $R_0$  is the dc resistance at reference temperature  $T_0$ ,  $T_c$  is the conductor temperature for  $R_c$  and  $\alpha$  is the temperature coefficient of the conductor material.

Consider a cylindrical shell of thickness  $dr$  as shown in Figure 3.1 where  $r_1$  and  $r_2$  are the radius of the conductor and insulation respectively. The temperature difference across  $dr$  is  $dT$ . The surface area of conductor is  $A_c = 2\pi r_1 L$ .

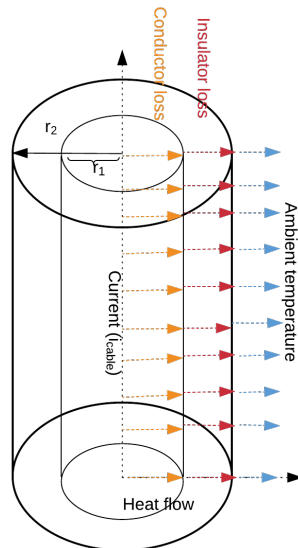


**Figure 3.1:** Heat transfer from conductor to the ambient

Certain assumptions are made in this thesis work when considering the thermal behaviour of cables as discussed below.

- The temperature difference along the cable length is not considered. Therefore, the heat flux along the length of the cable is neglected, i.e., ( $Q_{lengthdirection}=0$ )
- The heat transfer in the metallic screen (a small metal layer in-between the insulation layers) is not considered in this study since the metallic screen has a higher conductivity than the insulation. For simplification of the calculations, the temperature of the screen is taken to be the same as the conductor temperature.

According to Fourier's law, (3.1) can be integrated with respect to  $r$  from  $r = r_1$  at  $T = T_c$  to  $r = r_2$  at  $T = T_{amb}$  [25], according to

$$Q \int_{r_1}^{r_2} \frac{dr}{r} = -2\pi L k_{ins} \int_{T_c}^{T_{amb}} dT \quad (3.6)$$

where  $k_{ins}$  is the thermal conductivity of insulation. The heat rate equation is given by

$$Q = 2\pi k_{ins} L \frac{(T_c - T_{amb})}{\ln\left(\frac{r_2}{r_1}\right)} \quad (3.7)$$

where  $T_c$  is the cable surface temperature and  $T_{amb}$  is the ambient temperature. Equation (3.7) shows the variation of cable temperature over the cable surface according to the principles of heat transfer.

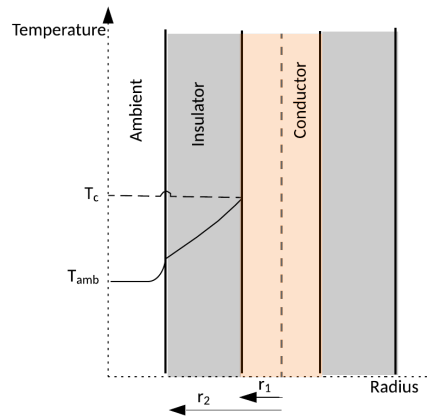


**Figure 3.2:** Temperature difference at cable cross-sections

Figure 3.2 shows the temperature distribution of the conductor and insulation of the cable as a function of its radius. The temperature at  $r_1$  is  $T_c$  and at  $r_2$  it is  $(T_c - T_{amb})$ . It is assumed that the conductor surface temperature is the same as the inner core temperature. There is a step deviation in the heat flux from the insulation surface to the ambient air having temperature  $T_{amb}$  due to the effective heat transfer coefficient  $h$  from (3.2). Therefore, the higher the temperature difference, the more heat power is transported [23].

### 3.1.2 Elements of LPN model

A simplified LPN (Lumped parameter network) thermal model of the cable is depicted in Figure 3.3.

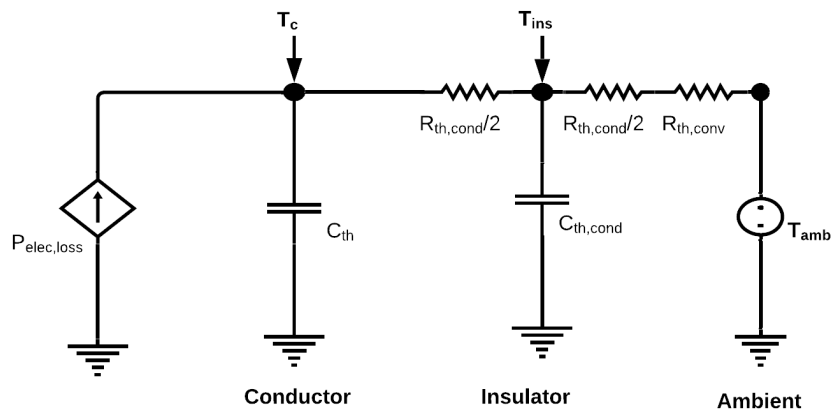


**Figure 3.3:** LPN model of the cable

The LPN model considers parts of the cable as lumped parameters, with radial heat transfer towards the outer surface of the cable into the ambient, as shown in Figure 3.1 [25]. This method gives a one-dimensional conduction analysis of the single-core cable [24]. In this study, the maximum conductor temperature  $T_c$  is calculated in order to determine the maximum permissible temperature of the insulation, in direct contact with the conductor.

The equivalent circuit consists of, conductor power loss as the source and the temperature nodes. The lumped parameters in the circuit given in Figure 3.3 are total thermal resistance of the cable ( $R_{th,tot}$ ), and the thermal capacitance ( $C_{th}$ ) [25], the capacitance of insulation ( $C_{th,cond}$ ) is neglected for simplicity of calculation, as the essential parameter is conductor temperature. In terms of the mass and specific heat, the thermal capacitance [26] can be given according to

$$C_{th} = mC_p \quad (3.8)$$

where  $m$  is the mass of the conductor and  $C_p$  is the specific heat capacity of the copper conductor. The mass of the conductor depends on the density of the copper and is given by

$$m = V_{cable}\sigma_{Cu} \quad (3.9)$$

where  $V_{cable}$  is the volume of the cable conductor and  $\sigma_{Cu}$  is the density of copper [ $kg/m^3$ ]. The volume of the conductor is given by

$$V_{cable} = A_c L \quad (3.10)$$

Further,  $R_{th,tot}$  according to Fourier's Law of heat conduction is given by

$$R_{th,cond} = \frac{\Delta x}{2\pi r_1 L k_{ins}} \quad (3.11)$$

where  $R_{th,cond}$  is the thermal resistance due to the insulation material,  $\Delta x$  is the thickness of the insulation material. The thermal conductivity  $k_{ins}$  increases with increase in cable conductor temperature  $T_c$ , thereby implying that  $R_{th,tot}$  also increases with an increase in  $T_c$ , as seen in (3.11). By considering convective cooling effects, the convective thermal resistance is now given by

$$R_{th,conv} = \frac{1}{hA_{ins}} \quad (3.12)$$

where  $R_{th,conv}$  is the thermal resistance due to convection (natural or forced),  $h$  is the heat transfer coefficient from (3.2) and  $A_{ins}$  is the area of the insulation surface and is given by  $2\pi r_2 L$ . With the convective heat transfer, the equivalent thermal resistance  $R_{th,tot}$  is calculated by combining (3.11) and (3.12) is given according to

$$R_{th,tot} = \frac{R_{th,cond}}{2} + \frac{R_{th,cond}}{2} + R_{th,conv} \quad (3.13)$$

$$R_{th,tot} = R_{th,cond} + R_{th,conv} \quad (3.14)$$

In Figure 3.3,  $P_{elec,loss}$  is the power supply to this thermal circuit and neglecting the  $C_{th,cond}$ . Thus applying Kirchoff's Current Law (KCL) to the circuit

$$-\frac{(T_c - T_{amb})}{R_{th,tot}} + P_{elec,loss} + \frac{T_c}{\frac{1}{sC_{th}}} = 0 \quad (3.15)$$

$$P_{elec,loss} = \frac{(1 + sR_{th,tot}C_{th})T_c - T_{amb}}{R_{th,tot}} \quad (3.16)$$

$$P_{elec,loss} = \frac{(sR_{th,tot}C_{th})T_c + (T_c - T_{amb})}{R_{th,tot}} \quad (3.17)$$

Applying inverse Laplace transformation to (3.17)

$$\frac{P_{elec,loss}R_{th,tot}}{C_{th}} = \frac{(T_c - T_{amb})}{C_{th}} + \frac{dT_c}{dt}R_{th,tot} \quad (3.18)$$

$$C_{th} \frac{dT_c}{dt} = P_{elec,loss} - \frac{(T_c - T_{amb})}{R_{th,tot}} \quad (3.19)$$

Equation (3.19) represents the ordinary differential equation to compute the temperature distribution by considering the lumped parameter formulation. The thermal power loss to the ambient is given by

$$P_{th,loss} = \frac{(T_c - T_{amb})}{R_{th,tot}} \quad (3.20)$$

where  $P_{th,loss}$  is the thermal power loss to the ambient. The temperature differential equation to be solved is given by

$$\frac{dT_c}{dt} = \frac{(P_{elec,loss} - P_{th,loss})}{C_{th}} \quad (3.21)$$

Substituting (3.8) in (3.21)

$$\frac{dT_c}{dt} = \frac{(P_{elec,loss} - P_{th,loss})}{mC_p} \quad (3.22)$$

Further simplifying (3.22) and substituting for  $P_{elec,loss}$  from (3.3) and  $P_{th,loss}$  from (3.20)

$$\frac{dT_c}{dt} = \frac{1}{mC_p} (i_{cable}^2 R_c - \frac{(T_c - T_{amb})}{R_{th,tot}}) \quad (3.23)$$

The electrical resistance  $R_c$  is obtained from (3.5) and in this case of 20°C reference temperature and cable length  $L$ , the cable resistance per unit metre is given by

$$R_c = R_{20}(1 + \alpha(T_c - (20 + 273.15))) \quad (3.24)$$

where  $R_{20}$  is the constant resistance at reference temperature 20°C. The resistance value keeps updating with the change in  $T_c$ . Thus the temperature differential equation to be solved is given by substituting for  $m$ ,  $R_c$ ,  $R_{th,tot}$

$$\frac{dT_c}{dt} = \frac{1}{mC_p} ((i_{cable}^2 (R_{20}(1 + \alpha(T_c - 293.15)))) - \frac{(T_c - T_{amb})}{R_{th,tot}}) \quad (3.25)$$

Equation (3.25) determines the maximum conductor temperature that is used to study the damage to the insulation material.

### 3.1.3 Fitting of thermal parameters to the data sheet

The geometrical parameters and the necessary material information is presented in the data-sheet (from Appendix). The cable manufacturer gives a constant value of thermal conductivity  $k_{ins}$  of the insulation material,  $k_{ins} = 0.23 [W/(m \cdot K)]$  and it is considered to be constant for a reasonable range of temperature changes. For varying current loads, the cable temperature exhibits a transient behaviour, which results in the variation of the  $k_{ins}$  value as well. Therefore, a method is developed to calculate  $k_{ins}$ , as shown in the following steps below.

#### Steps for determining $k_{ins}$ from the data-sheet:

- Create a few vectors of sample data points of current and temperature from the data-sheet. The values of temperature and current are re-traced from steady-state loading curve in the data-sheet.
- For a steady-state condition, (3.25) becomes

$$(i_{cable}^2(R_{20}(1 + \alpha(T_c - 293.15)))) - \frac{(T_c - T_{amb})}{R_{th}} = 0 \quad (3.26)$$

substitute  $R_{th,tot}$  in (3.11) in (3.26) gives

$$i_{cable}^2(R_{20}(1 + \alpha(T_c - 293.15))) - \frac{2\pi r_1 k_{ins}(T_c - T_{amb})}{\Delta x} = 0 \quad (3.27)$$

Find the value of  $k_{ins}$  from (3.27) for a known steady-state temperature from the data-sheet.

- Use the polyfit function in Matlab to fit the first-degree polynomial of the data, and evaluate the polyfit function in (3.28) to get the linear regression model of the data.

$$p = polyfit(T_c, k_{ins}, 1) \quad (3.28)$$

Specify two outputs to return the coefficients for the linear fit.

$$k_{ins} = p(1)T_c + p(2) \quad (3.29)$$

According to (3.29), first output coefficient (slope)  $p(1)$  is multiplied with  $T_c$ , in order to get the new  $k_{ins}$  value for each temperature iteration.

## 3.2 Ageing of Cables

The component durability study is significant to consider while designing the component. In HV cables, deterioration of the insulation material is a slow yet irreversible process caused by thermal stresses [17]. This section proposes a model to estimate the life of the cable due to thermal loading and also a damage value calculation which represents the reduction in the life of the cable.

### 3.2.1 Arrhenius ageing model

The insulation material is expected to withstand the thermal stresses within the cable. The extent of damage to the insulation properties is during transient overloads. And similarly, if an elevated temperature is applied continuously to the cable for an extended period, the cable insulation will be damaged [20]. Thus, an approach towards the failure of life analysis on the basis of time-varying thermal loading is proposed based on the Arrhenius ageing model. This model gives a realistic view of the impact of the thermal loading on the functional life of the cable.

The Arrhenius model evaluates and predicts the useful life of the cable insulation subjected to thermal stresses and environmental factors [20]. The Arrhenius equation in (3.30) for estimating the useful life of the cable is given by

$$L(T_c) = Ae^{B/T_c} \quad (3.30)$$

where  $L(T_c)$  is the useful life for a particular temperature,  $A$  &  $B$  are empirical constants and  $T_c$  is the conductor temperature.

#### 3.2.1.1 Determination of Arrhenius Constants

The empirical constants  $A$  and  $B$  in (3.30) are component specific parameters, whose values depends on the maximum operating temperature limits as shown in the Table 3.1.

**Table 3.1:**  $A$  and  $B$  parameters for the cable class

Wire Class	Min Temp limit [°C]	Upper temp limit [°C]	Temp to withstand for 240 hours [°C]	Temp to withstand for 6 hours [°C]
Class 1	-40	85	110	135
Class 2	-40	100	125	150
Class 3	-40	125	150	175
Class 4	-40	150	175	200
Class 5	-40	175	200	225
Class 9	-40	115	140	165

According to Table 3.1, the two conditions: 240 hours and 6 hours respectively, signifies the end-of-life of the cable for all classes when subjected to continuous loading at that applicable temperature limit. This implies the cable of a particular wire class, and for example, class 1 has an upper operating limit of 85°C. The HV cables experience transient current loading for a short interval, during which the conductor temperature goes above this mentioned limit. When a cable withstands a high thermal loading of 110°C continuously for 240 hours, then it reaches its expected life. Similarly, when subjected to thermal loading of 135°C continuously for 6 hours, the cable reaches its end-of-life. A novel method is proposed which utilises the two life conditions to estimate the parameters  $A$  and  $B$ .

The Arrhenius equation in (3.30) is modified by taking natural logarithm on both sides, to obtain a straight line equation  $y = m \cdot x + b$  form as given by

$$\ln(L(T_c)) = \frac{B}{T_c} + \ln(A) \quad (3.31)$$

The known quantities in (3.31) are the life of the cable and the maximum temperature withstand limit for 240 hours and 6 hours respectively. These conditions given in Table 3.1 are substituted in (3.31) and a linear regression is performed using polyfit in Matlab. The polyfit function computes the slope and intercepts for these two points in (3.31) given by  $m$  and  $b$  as coefficients respectively. Comparing (3.31) and  $y = m \cdot x + b$

$$polyfit = \left( \frac{1}{T_c}, \ln(L(T_c)) \right) \quad (3.32)$$

where the slope of (3.32) is  $m = B$  and intercept of (3.32) is  $b = \ln(A) \Rightarrow A = e^b$  and  $x = \frac{1}{T_c}$  in the line intercept equation. Thus the parameters  $A$  and  $B$  are obtained as in (3.32), and is calculated for each cable class similarly in the Arrhenius equation according to (3.30).

### 3.2.2 Damage Value

The damage value DV is the calculated relative loss of life of the cable due to thermal loading. For the cable component, damage is referred to as the time to failure in the presence of time varying thermal stresses and is computed using the Miner's rule. Miner emphasises that ageing accumulates over time where, transient thermal overloading is compensated by long periods of tolerable operating temperature of insulation [19]. According to Miner's rule shown in (3.33), damage value is the sum total of accumulated losses over the cable's entire life [19]. For  $i^{th}$  drive cycle the damage value is given by

$$DV_i = \lim_{\Delta t \rightarrow 0} \sum_0^t \frac{\Delta t}{L(T_c(\Delta t))} = \int_0^t \frac{dt}{L(T_c)} \quad (3.33)$$

where  $DV_i$  is the accumulated damage value for  $i^{th}$  drive cycle,  $\Delta t$  is the time spent at a particular cable temperature  $T_c$ ,  $L(T_c)$  is the life at the temperature  $T_c$  (3.30) [19] and  $[0 t]$  is the time period of the drive cycle. According to Miner's rule, in the presence of time-varying thermal loads, the accumulated damage value obtained from (3.33), reaches unity implying that the cable reaches its end-of-life [19].

Further from Miner's rule, the total relative damage value for a customer with  $N_{drivecycle}$  drive cycles is given by

$$DV_{tot} = DV_1 + DV_2 + \dots + DV_{N_{drivecycle}} \quad (3.34)$$

where  $DV_1, DV_2, \dots, DV_{N_{drivecycle}}$  are damage values for different drive cycles as obtained from (3.33).



# 4

## Method set-up

This chapter describes the generation of drive cycles and the cable current from the vehicle simulations. The method to solve the cable temperature differential equation is discussed, and the cable geometry and thermal parameters are tabulated. The life of the cable at various cable temperatures and the damage to the cable material properties are calculated, as discussed in Chapter 3. Further, the usage of the cables is investigated by defining a set of driver types and the share of their aggressive behaviour in each drive cycle. These driver types, combined with the frequency of occurrence, give a synthetic customer population. The following sections in this chapter describe the methodology for finding the usage of the 90<sup>th</sup> percentile customer and displaying their current cycles. This complete set-up using an algorithm-based approach in a Matlab script is summarised.

## 4.1 Overview of key procedures

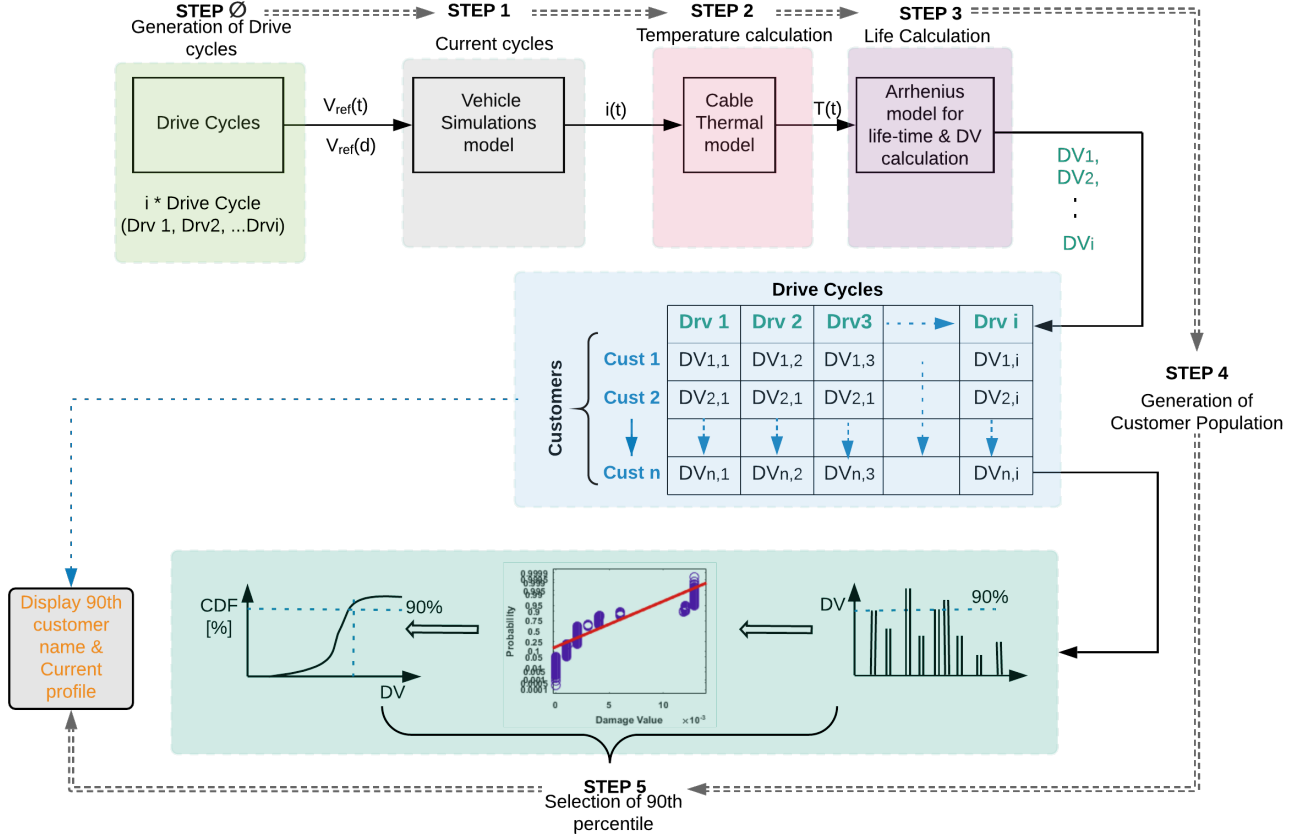


**Figure 4.1:** Methodology to select the 90<sup>th</sup> percentile customer

Figure 4.1 is a flow diagram of the main steps and they are :

- Step  $\phi$ :** Generation of drive cycles with reference speed  $v_{ref}(t)$  or  $v_{ref}(d)$ .
- Step 1:** Simulation of vehicle to obtain the current  $i(t)$ .
- Step 2:** Simulation of cable temperature  $T(t)$ .
- Step 3:** Calculation of the life of the cable for each drive cycle.
- Step 4:** Calculate relative damage for each drive cycle/driver type.
- Step 5:** Select the 90<sup>th</sup> percentile customer usage and display their current cycles.

## 4.2 Vehicle Simulations

An existing simulation model is used which corresponds to **Step 1** shown in Figure 4.1. VSim is a Matlab/Simulink based for vehicle simulations. The inputs for the simulation are the drive cycle and vehicle data such as the speed and acceleration profiles. The drive cycle is the set-point vehicle speed versus time. The output of

from the vehicle simulation is the cable current, shown in Figure 2.2, obtained for each drive cycle.

### 4.3 Cable Thermal model simulation

According to the principles of heat transfer discussed in Chapter 3.1, this section describes the detailed steps involved in calculating the temperature differential equation (3.25), corresponding to **Step 2** shown in Figure 4.1. Further, the cable dimensions and the material parameters used in the calculation are also discussed in this section. Figure 4.2 illustrates the procedure to simulate the cable temperature in (3.25) for the current profile obtained from vehicle simulations, as discussed in Section 4.2.

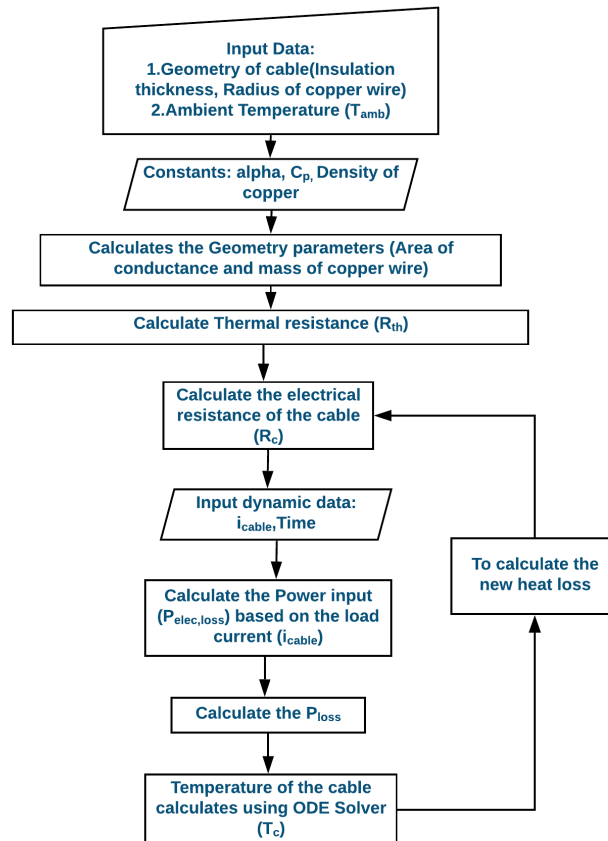


**Figure 4.2:** Temperature calculation flow chart

Initially, the input data such as the cable geometry and the ambient temperature are set according to Table 4.1.

**Table 4.1:** Initial parameters of the cable

Parameter	Value
Cross-sectional area( $A_c$ ) [ $m^2$ ]	$50 \cdot 10^{-6}$
Ambient Temperature [ $^{\circ}C$ ]	65
Radius of Insulation ( $50mm^2$ ) [ $m$ ]	$7.82 \cdot 10^{-3}$
Radius of Copper conductor ( $50mm^2$ ) [ $m$ ]	$3.99 \cdot 10^{-3}$
Radius of Insulation ( $35mm^2$ ) [ $m$ ]	$7.72 \cdot 10^{-3}$
Radius of Copper conductor ( $35mm^2$ ) [ $m$ ]	$3.33 \cdot 10^{-3}$
Radius of Insulation ( $70mm^2$ ) [ $m$ ]	$8.75 \cdot 10^{-3}$
Radius of Copper conductor ( $70mm^2$ ) [ $m$ ]	$4.72 \cdot 10^{-3}$

This is followed by defining the constants and the material parameters of the cable used in this study, according to Table 4.2.

**Table 4.2:** Material parameters of the cables investigated

Parameter	Value
Conductor Material	Copper
Insulation Material	Silicon Rubber
Specific Heat Capacity of copper $C_p$ [ $J/kgK$ ]	$0.39 \cdot 10^3$
Temperature Coefficient of Resistance [ $\alpha$ ]	$4 \cdot 10^{-3}$
$R_{20}$ Conductor Resistance at $20^{\circ}C$ ( $50mm^2$ ) [ $m\Omega/m$ ]	max. 0.368
$R_{20}$ Conductor Resistance at $20^{\circ}C$ ( $35mm^2$ ) [ $m\Omega/m$ ]	max. 0.527
$R_{20}$ Conductor Resistance at $20^{\circ}C$ ( $70mm^2$ ) [ $m\Omega/m$ ]	max. 0.259
Density of copper [ $kg/m^3$ ]	8960
Heat transfer coefficient of cable insulation towards surrounding [ $W/m^2K$ ]	40

The parameters in Table 4.1 and Table 4.2 are used to compute the mass of the cable from (3.9); thermal parameters:  $R_{th}$  from (3.11) and  $C_{th}$  from (3.8); electrical parameters :  $R_c$  from (3.24). The input parameter for the temperature calculation is the varying current loads,  $i_{cable}$  calculated from the battery from (2.1). The temperature differential equation given in 3.25 is solved using an *ode* solver. The *ode* solver is used to solve non-stiff or stiff calculations. In this study, *ode23* solver is used as a low order method to solve non-stiff differential equations. The syntax is given by

$$[t, T_c] = ode23(odefun, tspan, y0, options) \quad (4.1)$$

where *odefun* is the function handle which defines the functions to be integrated. The function  $dydt = odefun(t, T_c)$ , for a scalar  $t$  and cable temperature distribution  $T_c$ , will return a column vector  $dydt$  of data type absolute or decimal value that corresponds to  $f(t, T_c)$ . The *odefun* must accept both input arguments  $t$  and  $T_c$ , even if one of the arguments is not used in the function then *tspan* is given by  $[0 t]$ ,  $y0$  is the initial condition, and in this case it is the ambient temperature  $T_{amb}$ , *options* is a structure specified as a structure array. The *odeset* function is used

to create or modify the options structure of the *ode*. The *ode* solver interpolates the current and time vectors to obtain distinct points that make the computation faster and accurate. The resultant cable temperature  $T_c$  and the time  $t$  is updated by feed-forward to calculate the new electrical loss in the cable for the next current data point as input. The iteration repeats until the last current data point to obtain a distribution of temperature values. The temperature distribution is further used to estimate the life of the cable as discussed in detail in the next section.

## 4.4 Procedure for life and damage value calculation

This section corresponds to **Step 3** shown in Figure 4.1. The life of the cable utilised at every temperature interval  $L(T_c(\Delta t))$ , is calculated from the Arrhenius equation (3.2.1) and the accumulated damage value over an entire drive cycle is calculated from (3.33). The damage value per km driving for an  $i^{th}$  drive cycle is calculated according to

$$DV_{km,drivecycle,i} = \frac{DV_{drivecycle,i}}{d_{drivecycle,sim,i}} \quad (4.2)$$

where  $d_{drivecycle,sim,i}$  is the simulated drive cycle distance for the  $i^{th}$  drive cycle and  $DV_{drivecycle,i}$  is the damage value for the  $i^{th}$  drive cycle obtained by integrating the Arrhenius equation (3.2.1). The integration is performed using the trapezoidal function in Matlab and is given by  $trapz(t, L_c)$ . Equation (4.2) makes it easier to compute the damage value over any given distance to study the remaining life of the cable. Figure 4.3 depicts the flow of damage value calculation.

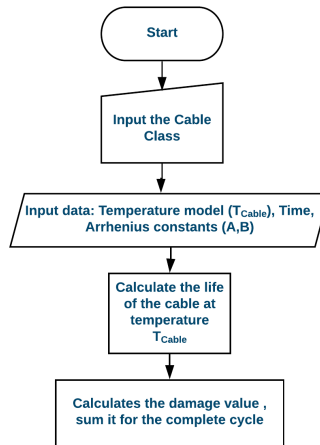


**Figure 4.3:** Calculation of damage value flow chart

The cable temperature distribution  $T_c$  is obtained from (4.1) by using the *ode* solver and is used in the Arrhenius equation given in (3.30) to calculate the life of the cable. The Arrhenius parameters  $A$  and  $B$  are calculated by the procedure given in Section 3.2 for the desired cable class, shown in Table 3.1. The integration

life of the cable is performed using the trapezoidal function in Matlab and is used to calculate the damage value for the cable. Thus the accumulated damage value over the entire utilised life of the cable is calculated based on the driving profile.

## 4.5 Generation of customers/drivers

This section describes the creation of the customer population for different drive cycles, corresponding to **Step 4**, as shown in Figure 4.1. The lifetime of an electrical component depends on customer usage in different drive cycles. Customer usage is defined by the drive type, driver behaviour and their frequency share of occurrence.

### 4.5.1 Basic drive cycles

The "basic" drive cycles corresponds to **Step  $\phi$**  shown in Figure 4.1. Basically, a drive cycle is a representation of the speed profile. There are two major types of drive cycles retrieved from the vehicle simulations, namely, distance-based drive cycles and event-based drive cycles. In this study, the cable currents are simulated for the different drive cycles as discussed in this section.

#### 4.5.1.1 Distance-based drive cycles

As the name suggests, a distance-based drive cycle is an actual model of the test on-road, where the reference speed is a function of distance  $v_{ref}(d)$ . In this study, different distance-based cycles are considered, namely, City, Highway, Mountain, Rural and Gravel. The vehicle reference speed, acceleration versus time of the distance-based cycles are presented in Figures 4.4 to 4.8.

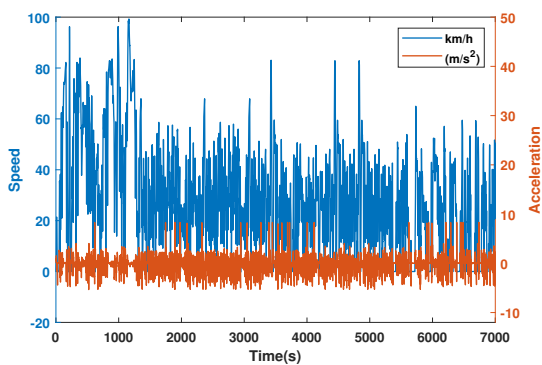


**Figure 4.4:** City drive cycle

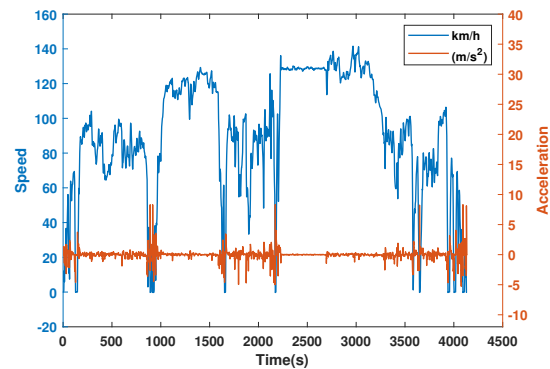


**Figure 4.5:** Highway drive cycle

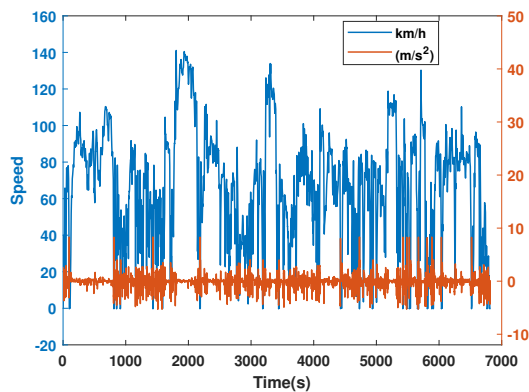


Figure 4.6: Mountain drive cycle

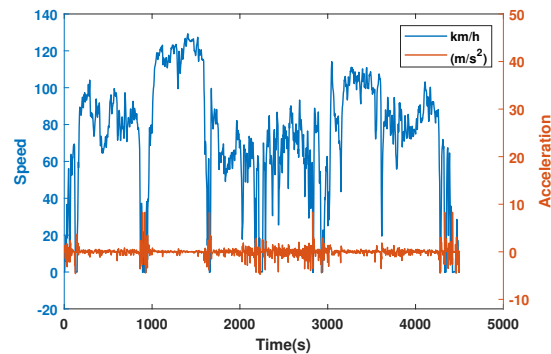


Figure 4.7: Rural drive cycle

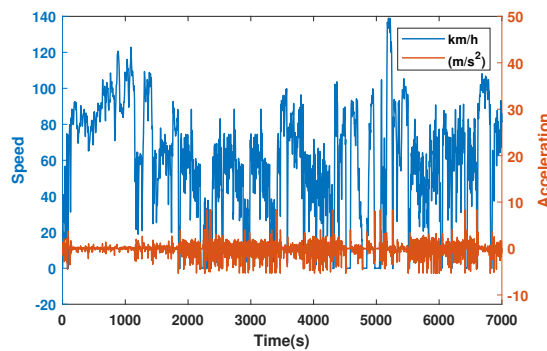


Figure 4.8: Gravel drive cycle

It is observed from Figure 4.4 that the city drive cycle shows the highest frequency of acceleration/braking events with an average speed of  $45.5 \text{ kmph}$  and a maximum speed of approximately  $85 \text{ kmph}$ . The highway drive cycle is seen in Figure 4.5 has a higher speed range when compared to the city cycle due to fewer acceleration/braking events. Figure 4.6 shows the Mountain cycle with frequent inclinations and slopes (grading force) and thus would require more power for the propulsion of the vehicle along the slopes. The mountain cycle has higher speed profile than the remaining drive cycles with a maximum speed exceeds  $120 \text{ kmph}$ . The rural drive cycle shown in Figure 4.7 follows a similar driving pattern as the highway drive cycle, but from  $t=2500 \text{ s}$  to  $t=5000 \text{ s}$  more acceleration/braking events are observed. For the gravel drive cycle shown in Figure 4.8, the average speed is approximately  $60 \text{ kmph}$  and has a frequent number of acceleration/braking events thus leading to higher current loads to propel the vehicle.

The drive cycles with a reference speed of  $v_{ref}(d)$ , exhibits different driver profiles, namely, aggressive, moderate, and mild. In these cycles, the cycle distance covered by each driver profile is the same, but their speed differs by a scaling factor  $k_{agg}$ , as seen in Table 4.3.

It is observed from Table 4.3 in a particular drive cycle, an aggressive driver having the highest speed covers the cycle distance  $d_i$  faster than the moderate

**Table 4.3:** Scaling factor for a drive cycle with different driver profiles

Driver Profile	Scaling factor ( $k_{agg}$ )
Aggressive	1.1
Moderate	1.0
Mild	0.9

and mild drivers. For example, if an aggressive driver with a reference speed of  $(1.1 \cdot v_{ref}(d))$  takes  $t_1$  s to cover a cycle distance of  $x$  km, then a mild driver with reference speed of  $(0.9 \cdot v_{ref}(d))$  would take  $t_2$  s to cover the same distance, and  $t_1 > t_2$ . The reference speed for a driver profile in a drive cycle is calculated according to

$$v_{ref,agg}(d) = k_{agg} \cdot v_{ref}(d) \quad (4.3)$$

where  $v_{ref,agg}(d)$  is the drive cycle's target or reference speed depending on the driver profile and  $d$  is the cycle distance of the drive cycle.

Table 4.4 presents the time difference taken to cover 94.28 km in a rural drive cycle based on the aggressiveness of a driver.

**Table 4.4:** Time and distance covered by the rural cycle

Drive Cycle	Driver Profile	Distance Covered [km]	Time taken [s]
Rural	Aggressive	94.28	4500
Rural	Moderate	94.28	4929
Rural	Mild	94.28	5455

It is observed from Table 4.4 that the rural aggressive driver with the highest speed covers 94.28 km in 4500 s, whereas the rural mild driver with the least speed takes 5455 s to cover the same distance. This behaviour is due to the difference in their reference speeds by a scaling factor  $k_{agg}$  according to Table 4.3.

#### 4.5.1.2 Event-based drive cycles

The event-based drive cycles are compressed models of the actual time taken to conduct the test on the road. These drive cycles are time-dependant where the reference speed is a function of time  $v_{ref}(t)$ . Typically, the tests are conducted on the autobahn and trailer drive cycles, independent of the driver profile. The event-based drive cycles are used for the vehicle simulations with defined conditions of maximum speeds and additional vehicle weights, as shown in figures below.

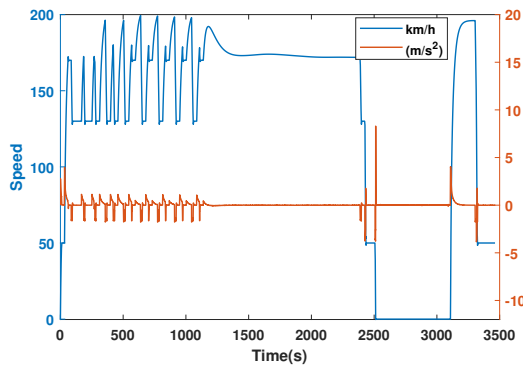


**Figure 4.9:** Autobahn drive cycle

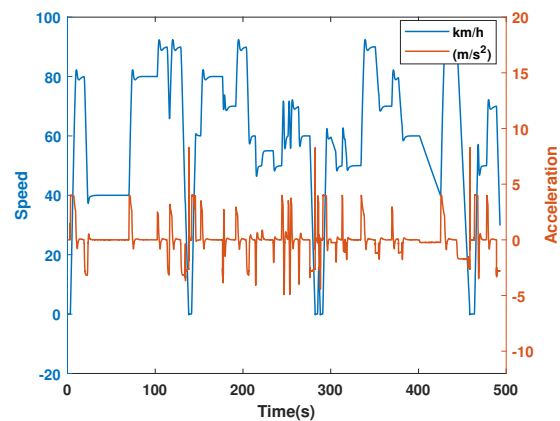


**Figure 4.10:** Trailer drive cycle

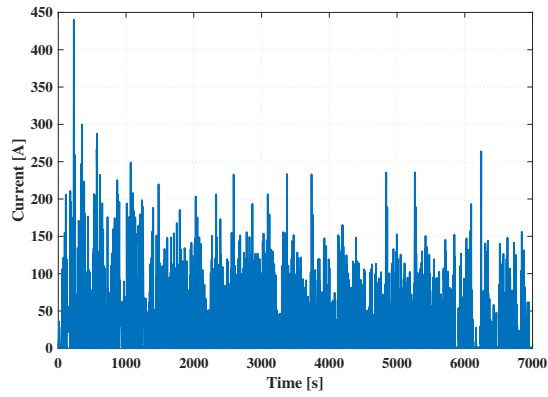
Figure 4.9 shows the simulated autobahn drive cycle with maximum speeds profile obtained from the vehicle simulations having an average speed of  $164 \text{ kmph}$ . In the autobahn drive cycle, the acceleration/braking intervals are observed only until  $t=1200 \text{ s}$  for the vehicle to reach the maximum speed. Once the vehicle reaches the top speed of  $180 \text{ kmph}$ , the speed is maintained to be a constant and there is zero acceleration for this duration. When the vehicle speed starts to drop at  $t=2350 \text{ s}$ , a sudden acceleration peak is observed, and as the speed decreases, the acceleration goes to zero. While Figure 4.10, shows the trailer drive cycle simulated for an added trailer weight of say  $W_{Trailer} = 2000 \text{ kg}$ , to the curb weight of the vehicle. It is observed that the trailer drive cycle has more acceleration intervals than the autobahn drive cycle, to overcome the friction due to the aerodynamic drag and the rolling resistance due to the added weight. The trailer drive cycle achieves a high speed of  $90 \text{ kmph}$  due to the acceleration/braking events within  $t=500 \text{ s}$ . Thus the higher the acceleration, the more torque is produced, and thereby more power is drawn from the traction battery. This results in higher currents (peaks) gained within a short duration for the event-based cycles. This results in higher currents (peaks) gained within a short time for the event-based cycles. By comparing the different types of drive cycles, it is observed that the event-based cycles occur for a shorter time period than the distance-based cycles.

## 4. Method set-up

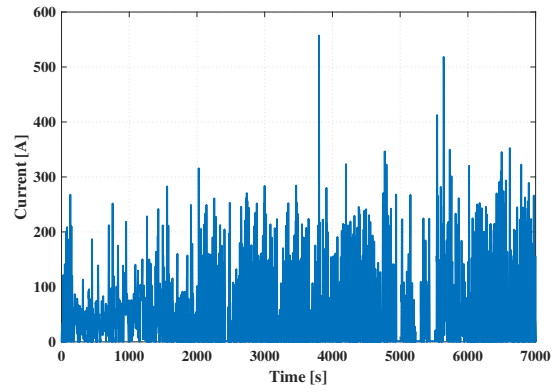
---

### 4.5.1.3 Simulated current for different drive cycles

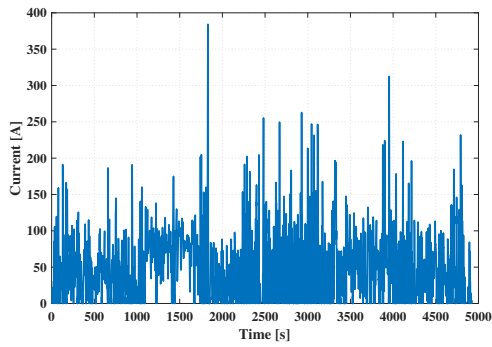
Figure 4.11 presents the simulated cable currents for a moderate driver in the different drive cycles which are obtained from the vehicle simulations.



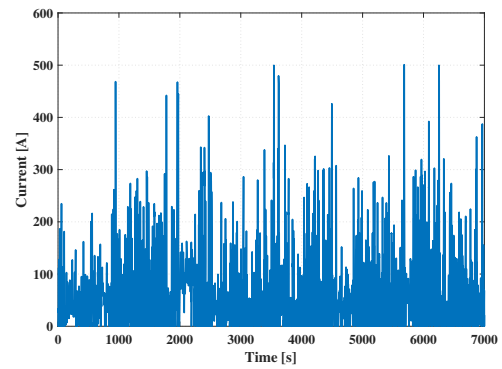
(a) City current cycle



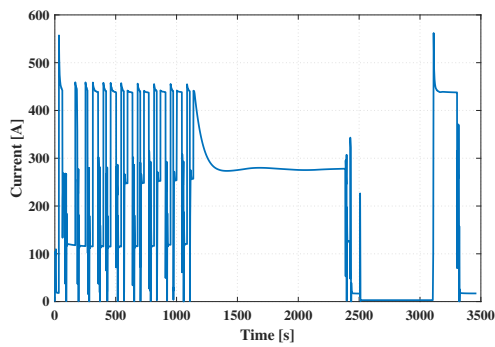
(b) Gravel current cycle



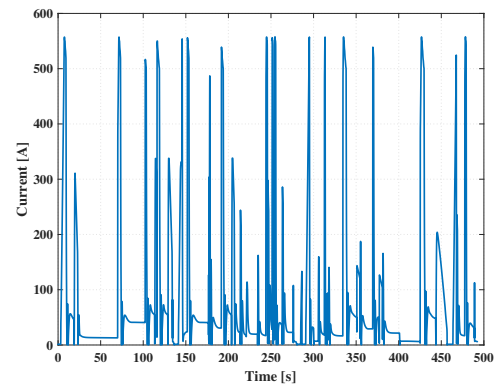
(c) Highway current cycle



(d) Mountain current cycle



(f) Autobahn current cycle



(g) Trailer current cycle

**Figure 4.11:** Current profiles for different drive cycles

Each drive cycle exhibits different driving profiles which directly impacts the reference speed and thus the current cycles as shown in Figure 4.11. Figure 4.11(a) shows the city current cycle, and it is observed that the peak current is 440 A. In the gravel current cycle shown in Figure 4.11(b), it is observed that the cable currents are higher than the city current cycle, with a peak current of 560 A and average current of 200 A. Figure 4.11(c) shows the highway current cycle with a peak current observed at 380 A, and the average current is 130 A. This current cycle is comparatively lower than the gravel and mountain current cycles. The current peaks are observed at many intervals to exceed 400 A for the mountain current cycle, as shown in Figure 4.11(d). The higher current cycles are due to frequent inclinations and braking events. In the case of the event-based cycles simulated for pre-defined conditions, Figure 4.11(f) shows the autobahn current cycles with a peak current of approximately 570 A; Figure 4.11(g) shows the trailer current cycle with a peak current exceeding 500 A. By comparing Figures 4.11(f) and 4.11(g), it is observed that the trailer current cycle achieves the same peak current as that of the autobahn current cycle within a short duration of 500 s. This is because the added trailer weight draws more power from the battery for the propulsion of the vehicle.

#### 4.5.2 Share of drive cycles for different driver types

The set of basic driver types  $N_{DrvType} = 20$  are distributed, as seen in Figure 4.12. Each driver type consists of  $N_{drivecycle}$  drive cycles and the name of the driver type reflects the maximum distance covered in a specific drive cycle.

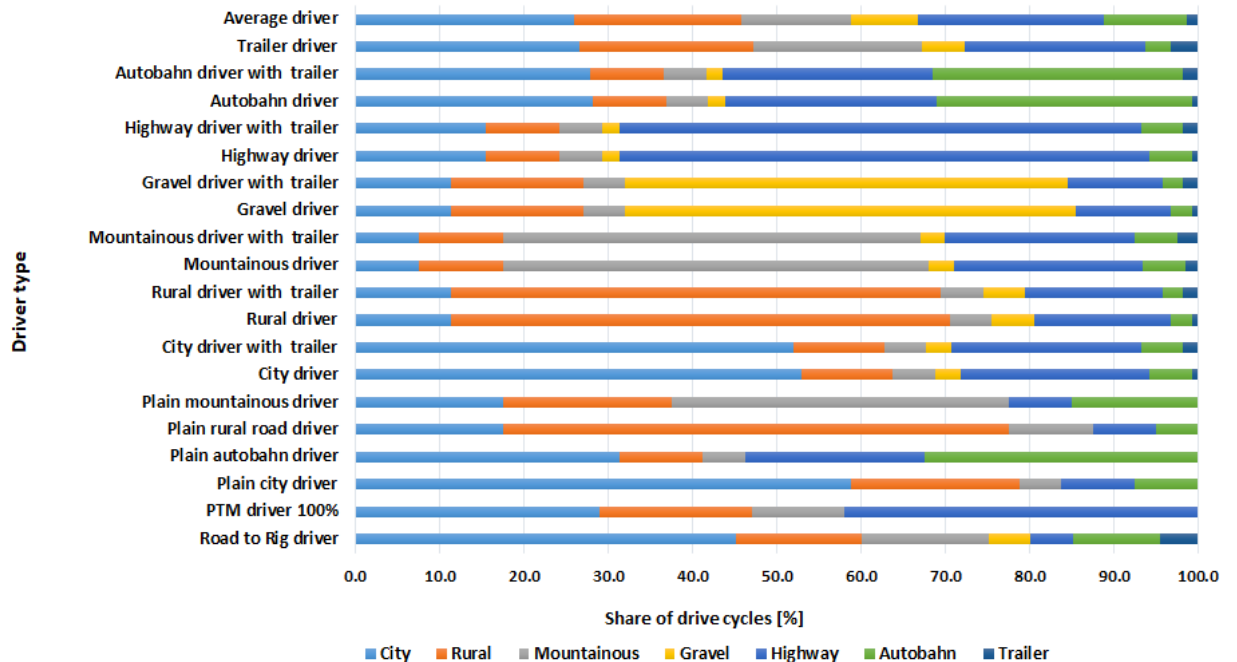


**Figure 4.12:** Distribution of  $N_{DrvType} = 20$  driver types based on their contribution in different drive cycles

For a driver type individual, the total damage value can be calculated using (4.2) and is given according to

$$DV_{tot,driver} = \sum_{i=1}^{N_{drivecycle}} DV_{km,drivecycle,i} \cdot d_{drivecycle,i} \quad (4.4)$$

where  $d_{drivecycle,i}$  is the total distance the driver drives in that very cycle. The total distance for an  $i^{th}$  drive cycle with an aggressiveness  $j$  can be calculated as

$$d_{drivecycle=i,agg=j} = d_{tot} \cdot r_{drivecycle=i} \cdot r_{agg=j} \quad (4.5)$$

where  $d_{tot}$  is the total distance covered by the  $i^{th}$  driver type and in this thesis a total mileage of 350000 km is assumed,  $r_{drivecycle=i}$  represents the percentage share of distance covered in that drive cycle and  $r_{agg=j}$  represents the aggressiveness of the speed profile in that drive cycle from (4.3).

From Figure 4.12, it is observed that for all driver types, the share in the trailer drive cycle is low compared to the remaining drive cycles. The trailer drive cycles have a rare occurrence in the real-time driving pattern. For example, a city driver type has a maximum share in the city drive cycle (53%) and least share in the trailer drive cycle (0.8%). The remaining drive cycles such as the highway cycle(22.5%), rural cycle(10.75%), mountain(5%) gravel cycle(3%) and autobahn(5%) have a moderate contribution. This shows that the City driver covers the maximum distance in the city cycle and the remaining distance in the other cycles.

As observed in Figure 4.12, the average driver drives have an average uniform share in most of the drive cycles. It can be observed that the driver types 'Road to rig driver' and 'Trailer driver' utilises much of the trailer cycle when compared to the other driver types. Similarly, the mountain and the highway driver types cover the maximum distance in their respectively named drive cycles. In this way, the drivers are named after their maximum share in a particular drive cycle.

### 4.5.3 Aggressiveness share for different driver types

Each driver type categorised in Figure 4.12 are further distributed according to their aggressiveness  $N_{agg} = 3$ , namely, aggressive, moderate and mild driver types as presented in Figure 4.13 below. The total number of driver types are given by,  $N_{DrvType,Beh} = (N_{DrvType} \cdot N_{agg}) = 20 \cdot 3 = 60$  driver types. For example, consider the distribution of a City driver type given in Section 4.5.2. The City driver type is further categorised into City Aggressive driver, City Moderate driver and City Mild driver, based on the driving behaviour.

Figure 4.13 shows that an aggressive driver is not always aggressive in a specific drive cycle. This driver is aggressive for the maximum share of distance covered in the drive cycle, i.e., an aggressive driver  $N_{agg} = 1$  is 40% aggressive, 50% moderate and 10% mild in a drive cycle. Similarly, a moderate driver  $N_{agg} = 2$  is moderate for 70% of the distance covered and 10% aggressive and remaining 20% mild and a mild driver  $N_{agg} = 3$  is 75% mild and is only 5% aggressive and 20%

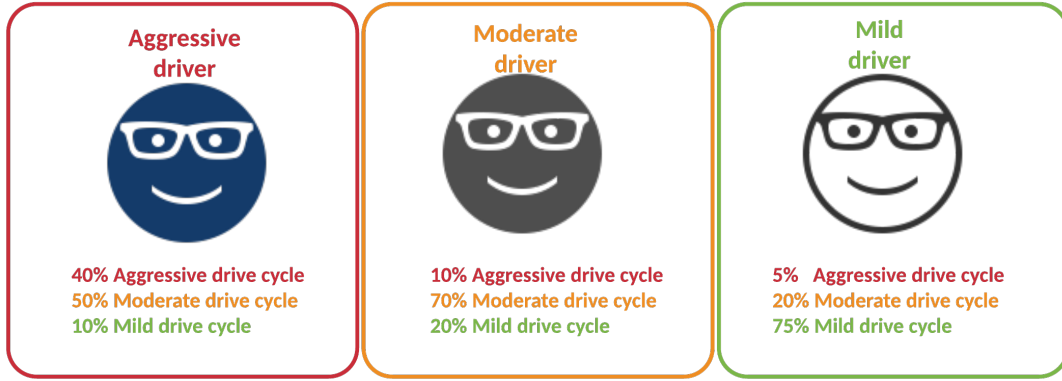


**Figure 4.13:** Behaviour share of different driver types

moderate for the total distance covered  $d_{tot}$  in the drive cycle. This is applicable to  $N_{DrvType}$  driver types categorised in Figure 4.12 to obtain the damage values of  $N_{DrvType}$  driver types. The damage value of a driver type with a defined driver behaviours  $N_{aggr}$  (aggressive, mild and moderate) is given according to

$$DV_{tot,drvertype,beh} = \sum_{i=1}^{N_{Drivecycle}} \sum_{j=1}^{N_{aggr}} DV_{km,drvcycle=i,aggr=j} \cdot r_{drvcycle=i} \cdot r_{aggr=j} \cdot d_{tot} \quad (4.6)$$

where  $r_{aggr=j}$  value depends on the aggressiveness of the driver type according to Figure 4.13, and  $N_{aggr} = 3$  for distance-based drive cycles and  $N_{aggr} = 1$  for event-based drive cycles. The drive cycle distribution for all different behaviours of a City driver is shown in Figure 4.14.

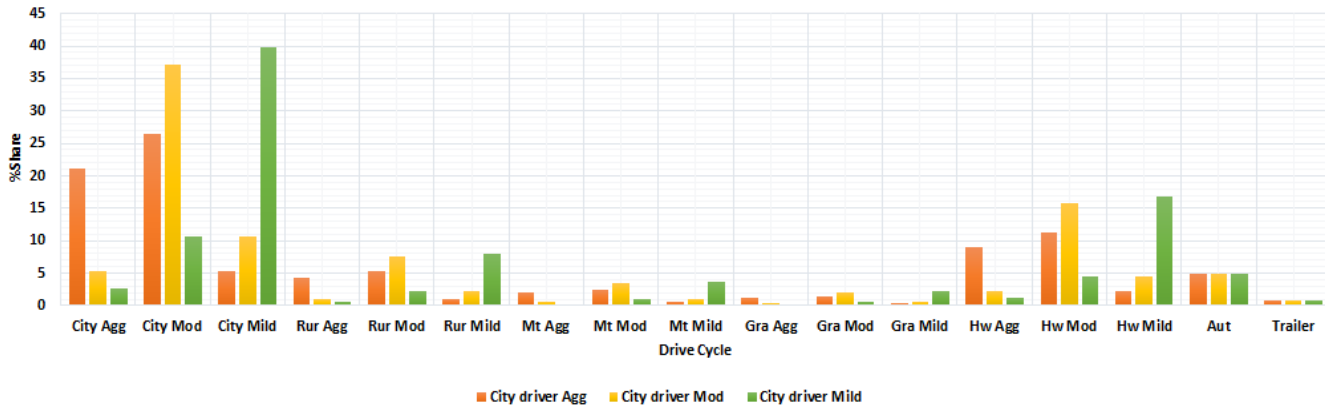


**Figure 4.14:** Share of drive cycles for aggressive, moderate and mild variants of the city driver type

It is observed that the percentage distribution of the city aggressive driver in the different drive cycles are not the same as the city moderate and city mild drivers, even though the initial drive cycle distribution is taken to be the same for all the three City driver types. For example, as discussed in Section 4.5.2, a city driver has a maximum driving share in the city drive cycle,  $M = 53\%$ . From Figure

4.13, the city aggressive driver is aggressive for  $(40\% \cdot M)$ , moderate for  $(50\% \cdot M)$ , and mild for  $(10\% \cdot M)$  of the distance covered in the city. Thus the accumulated damage value in the city drive cycle only is given by

$$DV_{city,agg} = DV_{km,city} \cdot M \cdot 0.40 + DV_{km,city} \cdot M \cdot 0.50 + DV_{km,city} \cdot M \cdot 0.50 \quad (4.7)$$

where  $DV_{city,agg}$  is the accumulated damage value of the city aggressive driver in the city drive cycle. Similarly, the accumulated damage of the city aggressive driver in the remaining drive cycles are calculated based on the percentage share in the respective drive cycles, and the total damage value is obtained for  $d_{tot} = 350000 \text{ km}$ . Thus it is observed from Figure 4.14 that the city driver covers a maximum distance in the city drive cycle and the percentage share of the driver depends on the driving behaviour in the drive cycle.

#### 4.5.4 Percentage share of total drivers

In this study, a synthetic population of customers are generated based on the recurrence of each driver type in the market. Initially,  $N_{DrvType} = 20$  different driver types are listed according to the usage in their respective environment, see Figure 4.12. The frequency occurrence of the  $N_{DrvType} = 20$  driver type are shown in the Figure 4.15.

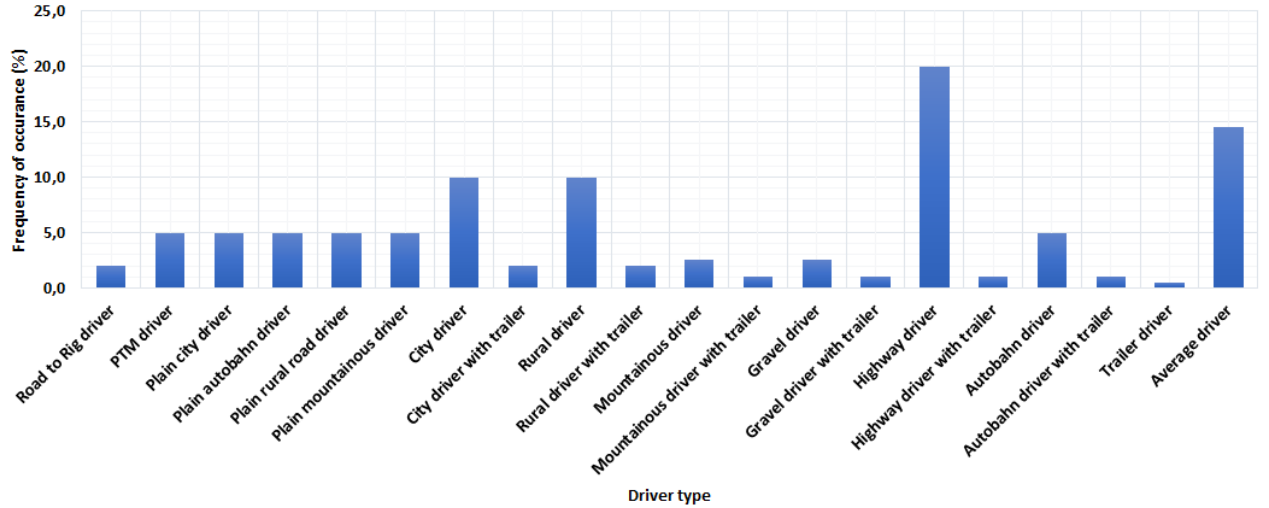


**Figure 4.15:** Percentage share of driver types based on occurrence

The frequency of occurrence means the number of times or the regularity with which the customer occurs in the total driver population. The Highway driver has the maximum frequency occurrence of (20%), followed by Average driver (15%). The Rural and City driver share the usage percentage of (10%). The least occurred driver profile is the Autobahn with Trailer, Highway with Trailer, Gravel with Trailer and Mountain with Trailer cycles of (1%). Summing up all the driver's percentage share is (100%).

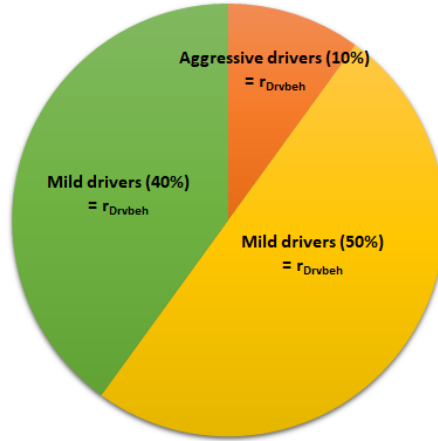


**Figure 4.16:** Population split of driver types

#### 4.5.4.1 Behaviour distribution in the customer population

Figure 4.16 shows the population split of each driver type based on the frequency of aggressiveness drivers. As part of customer generation, three different behaviours of drivers are considered (aggressive, moderate and mild), the behaviours of the driver is discussed in detail in Section 4.5.3. The total population split distribution is developed to obtain the number of drivers of each driver type in the total population. The moderate drivers contribute the majority of 50% to the population generation, followed by an aggressive driver with 10% and mild with 40%.

$$N_{DriverType} = N_{totCust} \cdot r_{DrvType} \cdot r_{Drvbeh} \quad (4.8)$$

where  $N_{DriverType}$  is the number of drivers of a particular driver type,  $r_{DrvType}$  is the frequency of occurrence of each driver type shown in Figure 4.12, and  $r_{Drvbeh}$  is the percentage of Aggressive, Moderate and Mild drivers as shown in Figure 4.16.

In this thesis, a total population of  $N_{totCust} = 2000$  customers is considered. For example, consider a city driver and driver type to be aggressive. The frequency occurrence of the city driver is 10%, and the share of aggressive drivers is 10% giving

$$N_{DriverType} = 2000 \cdot 0.10 \cdot 0.10 \quad (4.9)$$

$$N_{DriverType} = 20 \text{ drivers} \quad (4.10)$$

According to (4.8), the total number of city aggressive drivers are  $N_{DriverType} = 20$ .

## 4.6 Statistical method for selecting 90<sup>th</sup> percentile customer

This section briefly describes a statistical approach used to predict the lifetime of the cable component using the calculated damage values of the customer population,

as discussed in Section 4.5.4.1, corresponding to **Step 5** shown in Figure 4.1.

**Probability density function :** The probability theory is used to compute the up-time of the cable by defining a continuous random variable  $X$ , denoting the spectra of damage values and the probability distribution function (PDF)  $f_X(x)$  is defined as the point in time when the probability of a failure is likely to occur [19] and is according to [28] as

$$\int_{-\infty}^{\infty} f_X(x)dx = 1 \quad (4.11)$$

where  $x$  is a particular observed value of the random variable  $X$  and  $f_X(x)$  is the probability of  $X$  occurring at the given value of  $x$ . Thus the probability  $P$  that  $X$  is between the periods  $a$  and  $b$  is given according to [19] as

$$P(a \leq X \leq b) = \int_a^b f_X(x)dx \quad (4.12)$$

**Cumulative distribution function :** The cumulative distribution function (CDF)  $F_X(x)$  is a plot to display the percentile by plotting the percentage against the damage value. The CDF is the probability that  $X$  with a given PDF is likely to occur at a value lower than or equal to  $x$  and is given according to [28] as

$$F_X(x) = P(X \leq x) = \int_{-\infty}^x f_X(u)du \quad (4.13)$$

Figure 4.17 presents the cumulative distribution function for the damage values of the customer population.

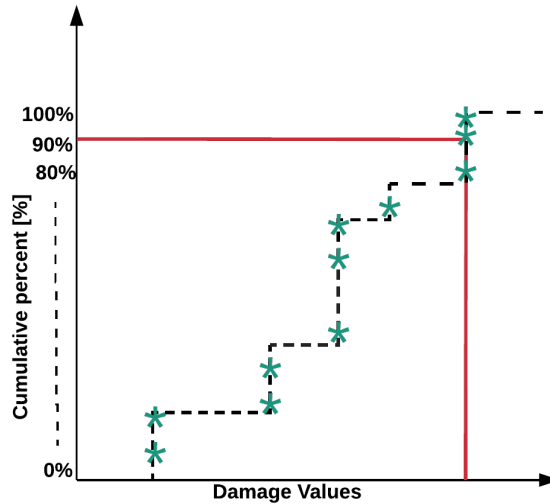


**Figure 4.17:** The cumulative distribution function for the damage value

The 90<sup>th</sup> percentile customer is selected by following the required steps.

1. Sort the damage values of the customers in ascending order.
2. Find the probability density function based on the frequency of occurrence of a

driver type as given in (4.11).

3. Find the damage value along the horizontal axis in the cumulative distribution function, given in (4.13).

4. Move vertically upward through the cumulative distribution function for the 90<sup>th</sup> percentile data point.

5. Move horizontally to the left and see the corresponding damage value from the sorted spectra.

6. If there are two points closer to the 90<sup>th</sup> percentile as shown in Figure 4.17, find the damage value which first exceeds 0.90. Thus the 90<sup>th</sup> percentile customer damage value is displayed along with its position index.

The current cycles, along with the hours of operation based on usage in each drive cycle, is determined for the 90<sup>th</sup> percentile customer from the cumulative distribution function.

## 4.7 Matlab script process flow

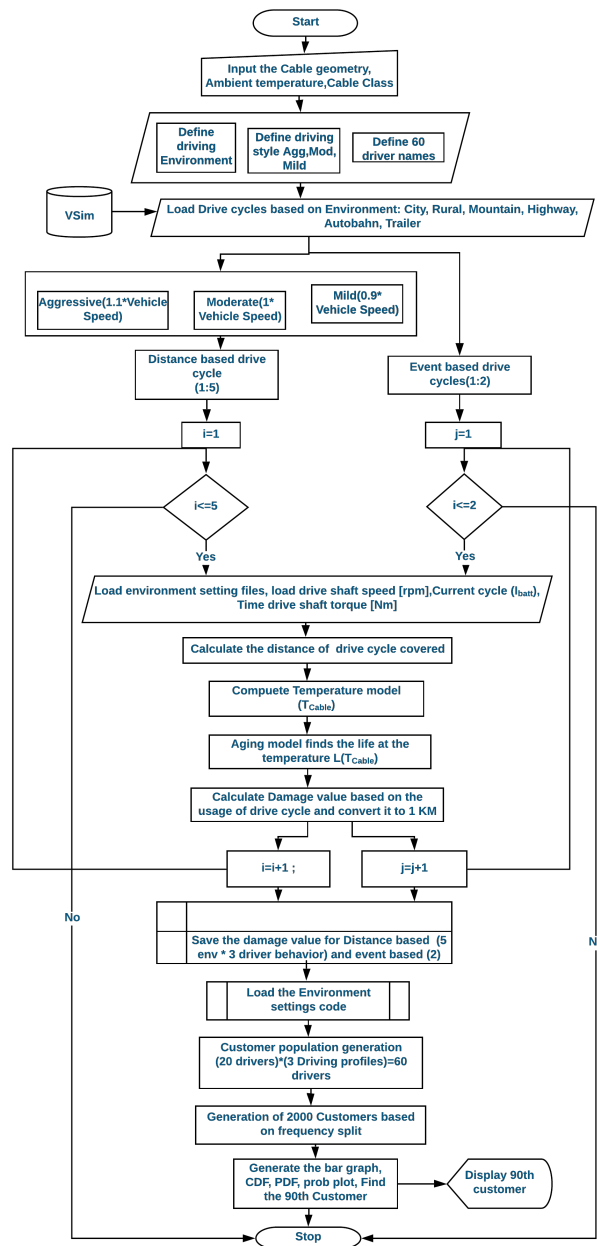


**Figure 4.18:** Complete flow diagram

An overview of the complete process flow for selecting the 90<sup>th</sup> percentile customer is shown in Figure 4.18.

**Step 1:** The cable geometry, ambient temperature and the temperature class for selection of best-fit cable are the input parameters.

**Step 2:** The drive cycles, driving behaviour and the driver names are defined in the Matlab script from 4.5.

**Step 3:** The drive cycles are loaded from the vehicle simulation. The drive cycles are City, Rural, Highway, Mountain, Autobahn and Trailer from Section 4.5.1.

**Step 4:** Define the scaling factor based on the driving behaviour and multiply this factor with the target speed of the drive cycle mentioned in the previous step from Section 4.5.1.

**Step 5 :** The process is repeated for the required iterations for the distance-based cycles (1:5) and event-based cycles (1:2)

**Step 6 :** Load the file containing the drive cycles distribution for the  $N_{DrvType}=20$  driver types based on their driving profile in each drive cycle from Section 4.5.2. Also, load their respective current cycles drawn from the HV Battery plant by the load. From this data, the time and the torque values are also retrieved to calculate the distance covered by each drive cycle.

**Step 7:** Compute the temperature distribution of the conductor considering the thermal parameters and the input parameters mentioned in **Step 1**.

**Step 8:** The life estimation model proposed in this study is used to calculate the useful life of the cable and the damage value calculation method is used to analyse the degradation of the insulation material from Section 3.2.1. The damage value spectra are computed for the usage of per km analysis for each drive cycle from Section 4.4. The per km value of each cycle is multiplied by the total mileage of  $d_{tot}=350000$  km to create a worst-case driving scenario.

**Step 9:** Save the damage value for the distance-based and event-based cycles after every iteration is complete.

**Step 10 :** The damage collective is computed for  $N_{DrvType,Beh}=60$  driver types from the initial  $N_{DrvType}=20$  driver types based on the driving behaviours  $N_{aggr}=3$  (aggressive, moderate or mild) as mentioned in **Step 2**, refer Section 4.5.3.

**Step 11 :** A synthetic customer collective of  $N_{totCust}=2000$  customers is created based on the frequency of occurrence of an individual driver type from Section 4.5.4.

**Step 12:** Statistical analysis of the damage values is obtained by evaluating the probability density function and the cumulative distribution function for the  $N_{totCust}$  customers' damage values. Thus, the 90<sup>th</sup> percentile customer is selected, and the name of the driver.

**Step 13:** The current profile is developed for the 90<sup>th</sup> percentile based on the drive cycle distribution. Based on the temperature generated from the current loading of this customer, the different cable classes are analysed, and the best-fit class is selected.



# 5

## Base Verification

This chapter verifies and validates the cable thermal model according to the cable datasheet (See Appendix A.1) as a reference.

### 5.1 Sensitivity of parameters with change in temperature

This section discusses the effect of change in the cable parameters on the calculated cable temperature at steady-state current loads. The input cable geometry and the material properties are used according to Table 4.1 and Table 4.2 in this section.

#### 5.1.1 Variation of thermal conductivity with conductor temperature

Figure 5.1 presents the variation in the thermal conductivity with the change in the conductor temperature.

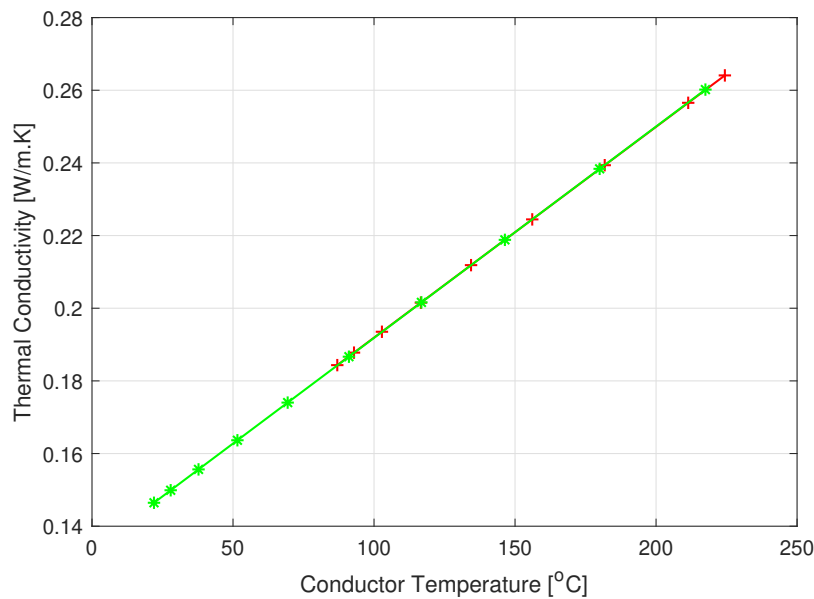


**Figure 5.1:** Calculated thermal conductivity of insulation  $k_{ins}$

The thermal conductivity of insulation  $k_{ins}$  is calculated according to (3.27) and fitted to data-sheet. It is observed from Figure 5.1 that for 20°C ambient temperature,  $k_{ins}=0.26$  at 217°C  $k_{ins}=0.14$  at 22°C and whereas for 85°C ambient temperature,  $k_{ins}=0.26$  at 224°C and  $k_{ins}=0.18$  at 87°C. Thus with increase in cable temperature the  $k_{ins}$  also increases proportionally.

### 5.1.2 Variation of thermal resistance with conductor temperature

Figure 5.2 shows the calculated thermal resistance  $R_{th,tot}$ , with only conduction ( $R_{th,cond}$ ) according to (3.11), and the effect of both conduction and high convective heat transfer on the total thermal resistance of the cable ( $R_{th,(cond+conv)}$ ) with  $h=40$ , according to (3.12).

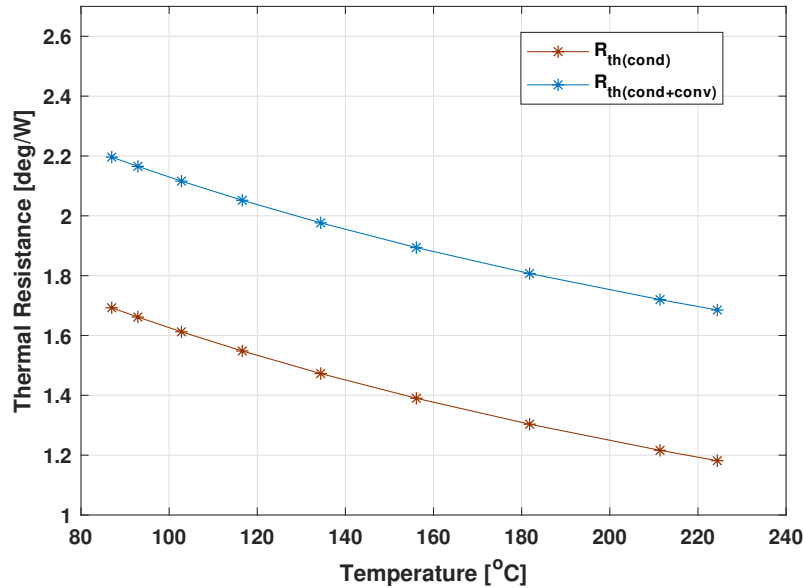


**Figure 5.2:** Calculated thermal resistance  $R_{th,tot}$  with and without convection

According to Figure 5.2, for a 50 mm<sup>2</sup> cable the cable conductor temperature is calculated using the parameters in Table 4.1 and Table 4.2. Considering conductive heat transfer,  $R_{th,cond}$  is 1.69 K/W at 87°C and with the increase in the conductor temperature to 224°C, the  $R_{th,cond}$  reduces to 1.18. Whereas, the total thermal resistance including convection  $R_{th,tot}$  is 2.19 K/W at 87°C and reduces gradually with increase in temperature. Therefore, two observations are deduced from the figure above. Firstly, the thermal resistance  $R_{th,tot}$  decreases with the increase in the conductor temperature, given that  $R_{th,tot}$  is inversely proportional to the thermal conductivity  $k_{ins}$ , see Figure 5.1. Secondly, including the convective heat transfer coefficient increases the total thermal resistance  $R_{th,tot}$  which will eventually result in less damage to the insulation properties. This can be validated from Table 5.1 below.

**Table 5.1:** Calculated thermal resistance  $R_{th,cond}$  and  $R_{th,(cond+conv)}$ 

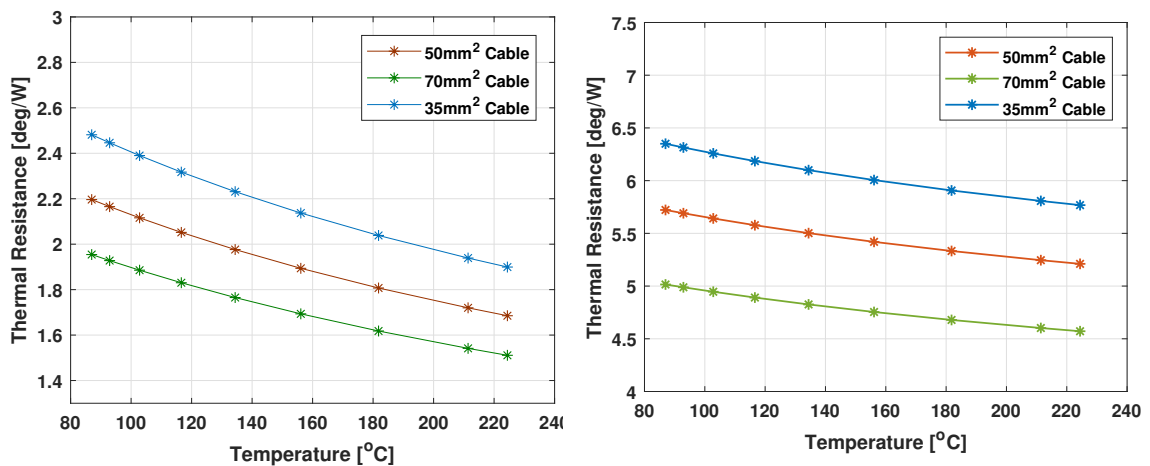
Temperature [°C]	86.9	102.8	134.4	181.2	224.4
$R_{cond}[K/W]$	1.69	1.61	1.47	1.30	1.18
$R_{cond+conv} [K/W]$	2.19	2.11	1.97	1.80	1.68

Table 5.2 and Figure 5.3 shows the calculated total thermal resistance  $R_{th,tot}$  for varying heat transfer coefficient where  $h=5$  for poor convective cooling and  $h=40$  for very high air flow with varying conductor geometry.

**Table 5.2:** Calculated thermal resistance  $R_{th,tot}$  with change in geometry

Temperature [°C]	86.9	102.8	134.4	181.2	224.4
$R_{th,tot(cond+conv)}(h=40)(70mm^2) [K/W]$	1.95	1.88	1.76	1.61	1.51
$R_{th,tot(cond+conv)}(h=40)(50mm^2) [K/W]$	2.19	2.11	1.97	1.80	1.68
$R_{th,tot(cond+conv)}(h=40)(35mm^2)[K/W]$	2.48	2.39	2.23	2.03	1.89
$R_{th,tot(cond+conv)}(h=5)(70mm^2) [K/W]$	5.01	4.94	4.82	4.67	4.57
$R_{th,tot(cond+conv)}(h=5)(50mm^2) [K/W]$	5.72	5.64	5.50	5.33	5.21
$R_{th,tot(cond+conv)}(h=5)(35mm^2) [K/W]$	6.34	6.25	6.09	5.90	5.76

The cable parameters are used according to Table 4.1 to calculate the thermal resistance  $R_{th,tot}$  for different cable geometry. For poor cooling, a  $h$  factor of 5 [ $W/m^2 \cdot K$ ] is taken. It is observed that at 87°C, for a 70  $mm^2$  cable  $R_{th,tot} = 5.01$  and it increases to  $R_{th,tot} = 5.72$  for a 50 $mm^2$  cable. But, a reduced value of  $R_{th,tot}$  is observed when a  $h$  factor of 40 [ $W/m^2 \cdot K$ ] is considered in the case of forced air cooling, according to Table 5.2. Thus, with an increase in cable surface area effective heat transfer to the ambient air takes place, as shown in Figure 5.6.

**Figure 5.3:** Calculated thermal resistance  $R_{th,tot}$  with change in geometry for  $h=40$  and  $h=5$

### 5.1.3 Temperature model for steady-state current

In this study, simulations are carried out under the assumption that the system is has continuous current loading, and the temperature at the conductor is constant. Table 5.3 presents the validated temperature model developed in Matlab in reference to the cable datasheet A.1.

**Table 5.3:** Comparison of conductor temperature output of datasheet and simulated results

Current [A]	100	200	300	400
Simulated Temperature [ $^{\circ}C$ ]	92.9	116.7	156.3	211.8
Data Sheet Temperature [ $^{\circ}C$ ]	92.9	116.6	156.1	211.4

Figure 5.4 shows the calculated conductor temperatures for steady-state current steps of 100 A, 200 A, 300 A and 400 A and a time period of  $t= 3600$  s at an ambient temperature of  $85^{\circ}C$ , according to (3.25) in Section 3.1.2 and the input parameters are A.1.

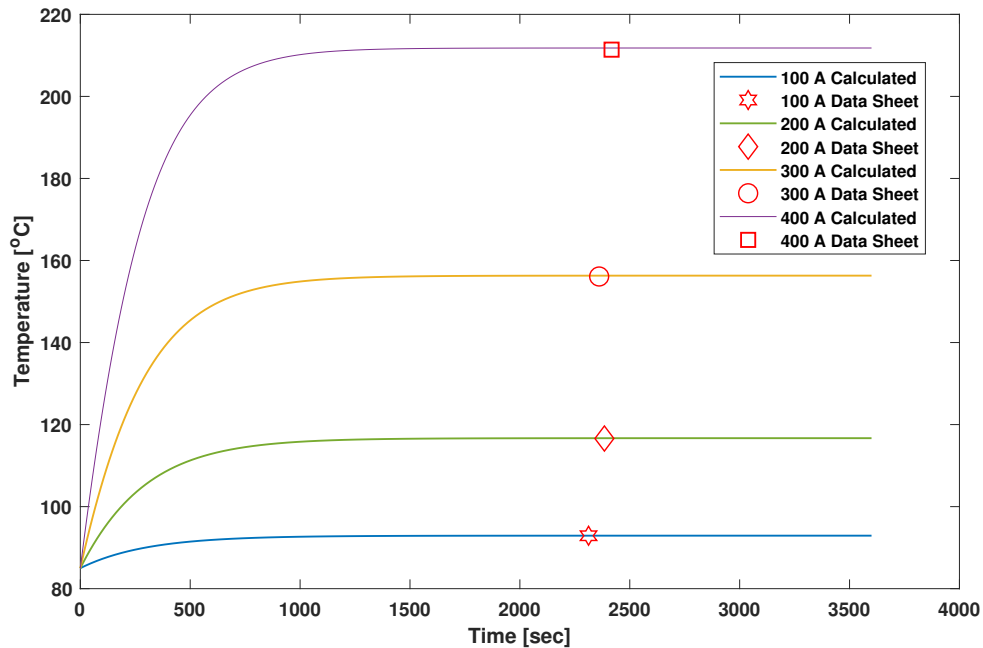


**Figure 5.4:** Calculated conductor temperature plot for steady-state continues current steps for  $85^{\circ}C$  ambient temperature and  $50mm^2$  cable

From Figure 5.4 it is observed that when operating the cable at a steady-state load current of 400 A, the conductor temperature is nearly  $212^{\circ}C$ , and the conductor is in a stable thermal equilibrium once the temperature reaches the steady-state. The temperature plot for steady-state currents is compared with the data-sheet to validate the model, shown according to Table 5.3 above. And the results

shows that both the models follows the same conductor temperature response for the steady-state current steps. The calculation code of the cable conductor temperature is presented in A.2.3.1.

**Calculation of conductor temperature  $T_c$  for steady-state current:**

- For a steady-state condition, (3.25) becomes

$$i_{cable}^2(R_{20}(1 + \alpha(T_c - 293.15))) - \frac{(T_c - T_{amb})}{R_{th}} = 0 \quad (5.1)$$

$$T_c = i_{cable}^2(R_{20}(1 + \alpha(T_c - 293.15)))R_{th} + T_{amb} \quad (5.2)$$

$$R_c = R_{20}(1 + \alpha(T_c - 293.15)) = 4.664 \cdot 10^{-4} \quad (5.3)$$

where  $R_{20}=0.368 \cdot 10^{-3}$ ,  $\alpha=4 \cdot 10^{-3}$ ,  $T_{amb}=85^\circ\text{C}$ , taking  $T_c$  value close to ambient conditions  $87^\circ\text{C}$ , and substituting  $R_{th}=1.69$  for  $87^\circ\text{C}$  from Table 5.1 in (5.2). The calculated conductor temperature for  $i_{cable} = 400 \text{ A}$  from (5.2) is  $211.13^\circ\text{C}$  which follows the simulated values obtained in Table 5.3.

### 5.1.4 Time to reach steady-state

According to Table 5.4 for steady-state current loads, the time taken to reach 230°C of conductor temperature is validated with the cable datasheet A.1.

**Table 5.4:** Comparison of calculated time to reach 230°C by cable conductor to the simulated results and data-sheet

Current [A]	2000	4000	6000	8000
Simulated Time [s]	11.4	2.8	1.2	0.7
Data Sheet Time [s]	10.8	2.7	1.2	0.7

Figure 5.5 shows the calculated time to reach 230°C for the steady-state loads at 85°C ambient temperature, according to (3.25).

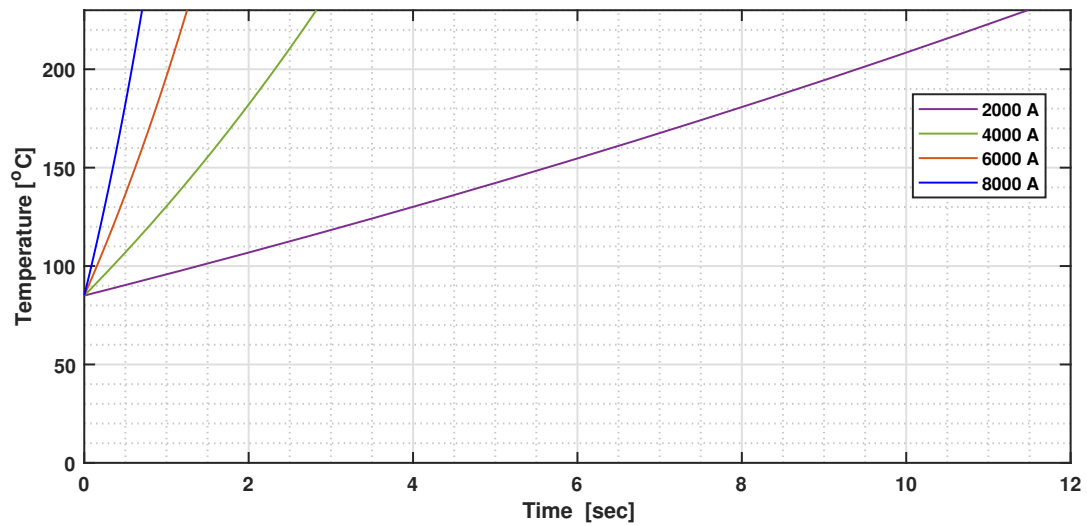


**Figure 5.5:** Calculated time to reach 230°C of cable conductor for the current loads with an ambient temperature of 85°C

As expected, the time to reach 230°C decreases with increasing load current. The simulated results closely agree with the datasheet values.

### 5.1.5 Influence of heat transfer coefficient on conductor temperature

Figure 5.6 presents the difference in the conductor temperature response, with natural, poor and forced air flow cooling.

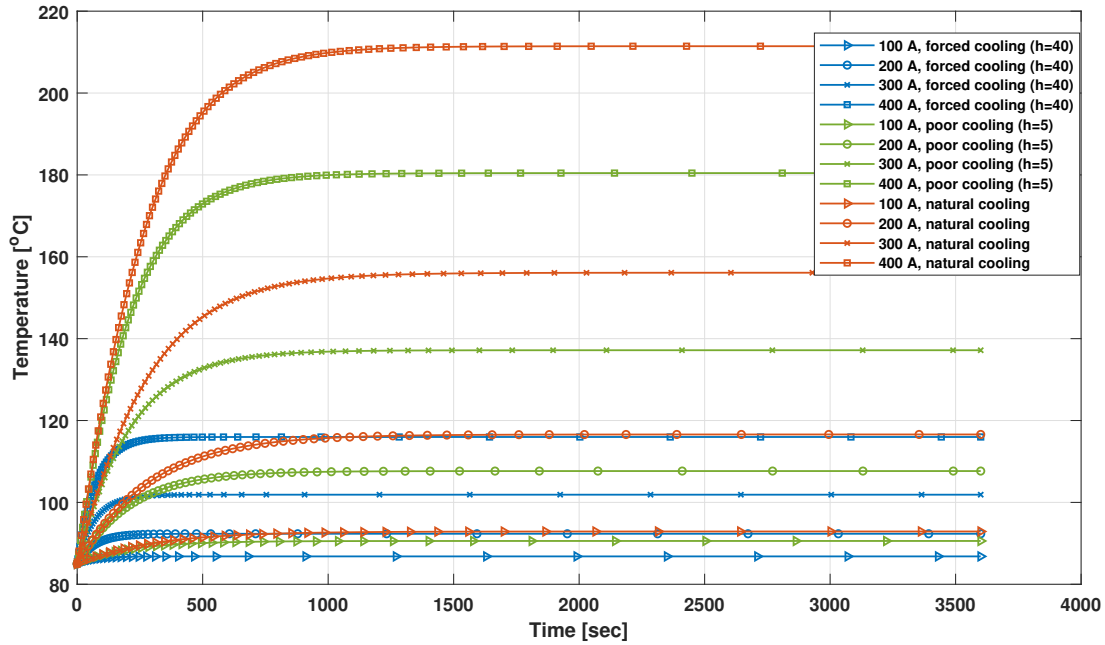


**Figure 5.6:** Calculated conductor temperature with step current loads for with natural, poor and forced convective cooling at an ambient temperature of 85°C

The calculated conductor temperature according to (3.25) is simulated for an extreme-case ambient temperature of 85°C and steady-state current steps. It is perceived that with natural convective cooling (assumed as cooled only with ambient condition as in a closed chamber, so  $h$  value is neglected) the temperature for a current step of 400 A is 212°C, and the cable conductor temperature decreases with the poor convective cooling ( $h=5$ ) to 180 °C for the same current step, further with the forced convective cooling ( $h=40$ ) the conductor temperature reduces to 116 °C. Thus, with forced convective cooling for a 50 mm<sup>2</sup>, the cable reaches a lower conductor temperature for the same step current. Also, the variation between the value of the conductor temperature for with natural and forced convective cooling shows a higher variation for a 400 A current step with a temperature difference of 95°C whereas the temperature difference of 6°C for a 100 A current step.

### 5.1.6 Impact of change in conductor geometry on cable temperature

Figure 5.7 shows the calculated conductor temperature according to (3.25), for current steps and different cross-sectional areas of the conductor, at an ambient temperature of  $85^{\circ}\text{C}$ .

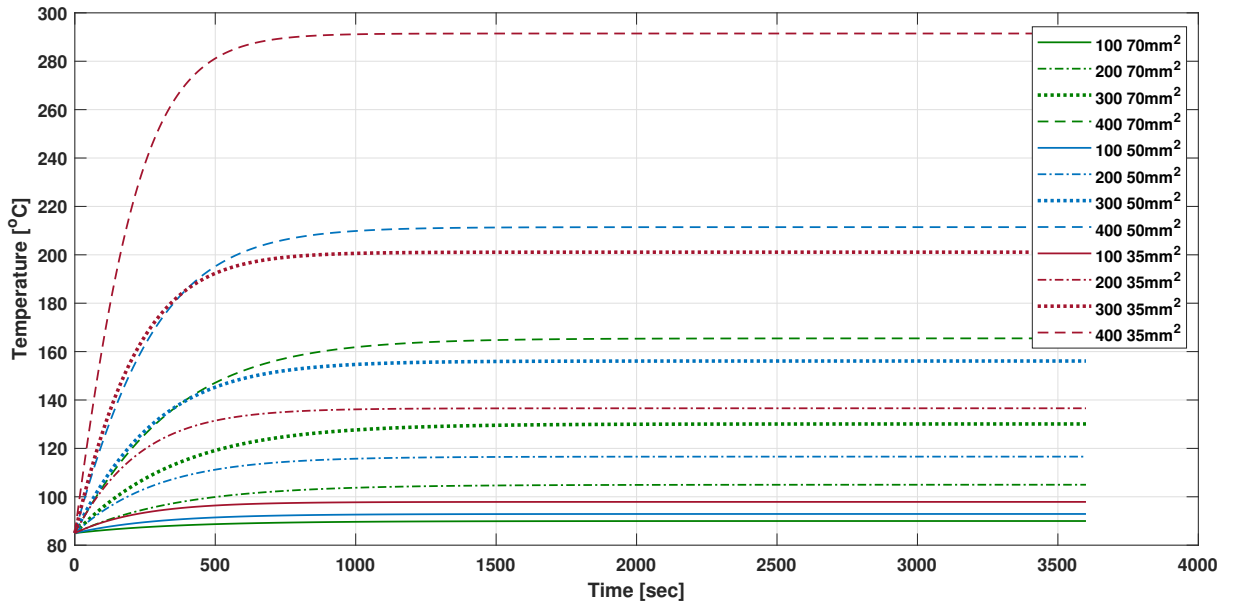


**Figure 5.7:** Calculated conductor temperature with step current loads for different cross-sections of cables at the ambient temperature of  $85^{\circ}\text{C}$

It is observed that with for a given cross-sectional area of the conductor, the cable temperature increases with an increase in the current load. But with an increase in the surface conductor area, the conductor temperature decreases due to the decrease in  $R_c$  according to (3.4). Thus a  $35 \text{ mm}^2$  cable reaches a very high cable temperature of approximately  $292^{\circ}\text{C}$  at  $400 \text{ A}$  whereas a  $70 \text{ mm}^2$  cable reaches  $165^{\circ}\text{C}$  for the same load. According to the datasheet, the desired operating temperature limit for the cable is approximately  $180^{\circ}\text{C}$ , and so a  $50 \text{ mm}^2$  or  $70 \text{ mm}^2$  cable is more suitable than the  $35 \text{ mm}^2$  cable. In this thesis, a  $50 \text{ mm}^2$  cable is selected to predict the life of the cables based on the usage.

# 6

## Analysis

In this chapter, the influence of the different drive cycles and driving behaviours on the calculated conductor temperature for a  $50 \text{ mm}^2$  cable is studied in detail. The conductor temperature analysis is carried out considering only heat conduction in the cables. The data from this analysis is used to calculate the life of the cable and thus to find the damage value. The method developed to generate the customer population, discussed in Section 4.5, is utilised to analyse the damage value for each driver type and also the best-fit cable class. The 90<sup>th</sup> percentile customer is selected based on the damage value spectra, and the current cycles along with the number of drive cycle repetitions are presented for the specific customer. The effect of varying ambient conditions and convective cooling for the 90<sup>th</sup> percentile customer is investigated. Furthermore, the impact of mileage accumulation and fast charging profile at different charging rates on the life of the cables is analysed based on the duration of the trip.

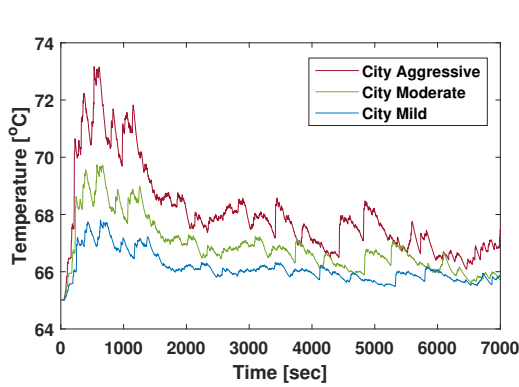
### 6.1 Cable thermal analysis for different drive cycles

The resulting figures discussed below gives a detailed analysis of the conductor temperature behaviour due to the current loading based on the usage in different drive cycles and also the impact of the driving behaviour. The simulations are carried out for the  $50 \text{ mm}^2$  according to Table 4.1 and Table 4.2 at an ambient temperature of  $65^\circ\text{C}$ .

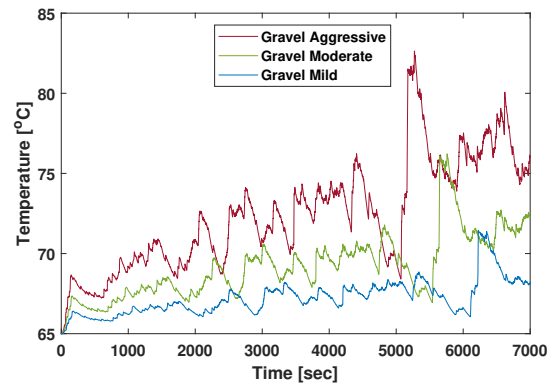
#### 6.1.1 Temperature determination for distance-based cycles

Figure 6.1 shows the calculated conductor temperatures according to (3.25) for different drive cycles and driver behaviours of the distance-based cycles.

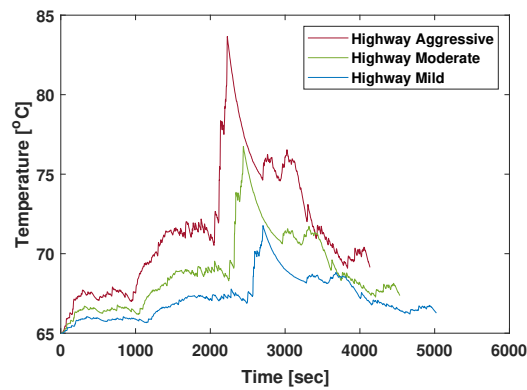
## 6. Analysis



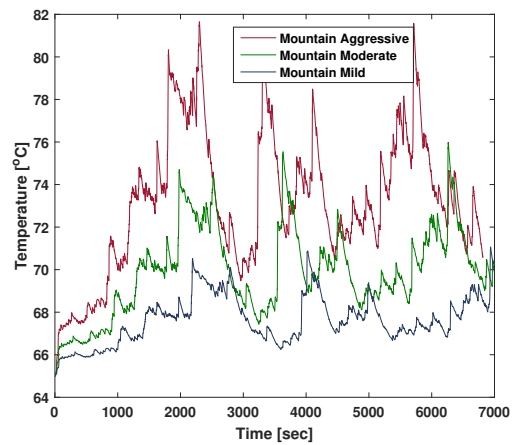
(a) City drive cycle



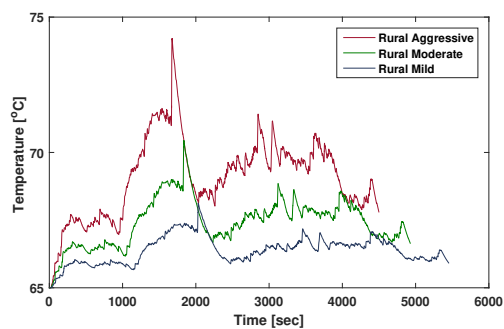
(b) Gravel drive cycle



(c) Highway drive cycle



(d) Mountain drive cycle



(e) Rural drive cycle

**Figure 6.1:** Thermal model response to the current loading (distance based cycles)

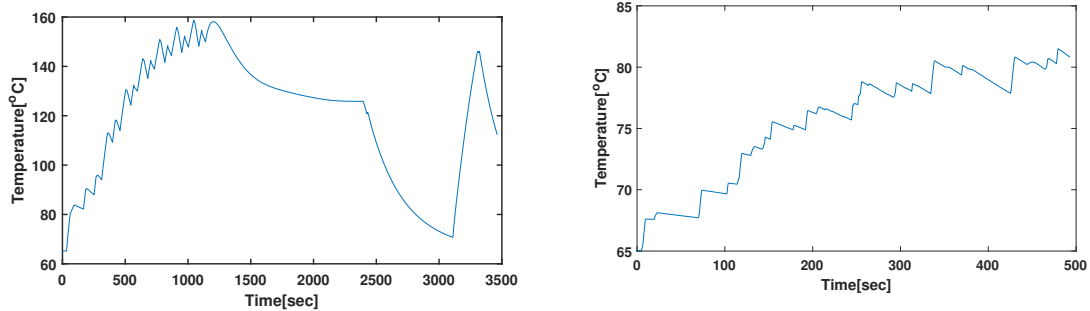
According to Figure 6.1, it is observed that the aggressive cycles have higher cable temperatures than the mild cycles. The city aggressive cycle presented in Figure 6.1(a) has a maximum temperature of  $73^{\circ}\text{C}$  at the time of  $700\text{ s}$ , and it is

due to the high current loading of 440 A from the current plot as shown in Figure 4.11. In the gravel aggressive cycle presented in Figure 6.1(b), the temperature gradually increases and reaches up to 83°C. The highway aggressive cycle presented in Figure 6.1(b) has the maximum of 84°C and fewer variations compared to the city and gravel cycle due to less acceleration observed in Figure 4.5. The mountain cycle presented in Figure 6.1(d) has substantially more spikes in the conductor temperature compared to the highway cycle, due to high slopes which loads the electric drive train.

Another essential aspect to categorise the behaviour could also be noted in Figure 6.1. The aggressive drive cycle results in temperature peaks in all driving cases before the moderate and the mild drivers. Figure 6.1(e) shows that the aggressive driver finishes the complete cycle before the moderate and mild drivers.

### 6.1.2 Temperature determination for event-based cycles

Figure 6.2 shows the temperature plot for the event-based cycles, namely autobahn and trailer.



(a) Autobahn drive cycle

(b) Trailer drive cycle

**Figure 6.2:** Thermal model response to the current loading (event based cycles)

It is observed from Figure 6.2 that the autobahn drive cycle has a peak current at 158°C, but the cable temperature for the trailer drive cycle gradually increases with increase in acceleration over time, see Figure 4.10. Thus from this figure, it is observed that the event-based cycles reach higher temperature peaks within a short period when compared to the distance-based cycles. So a high usage of this type of drive cycles could accelerate the ageing of cables compared to the normal usage.

### 6.1.3 Arrhenius ageing model for drive cycles

The ageing of the cables is analysed according to Section 3.2. The constants  $A$  and  $B$  are computed according to the method discussed in Section 3.2.1.1. Table 6.1 presents the calculated ageing constants  $A$  and  $B$  for the different cable classes.

#### 6.1.3.1 Arrhenius parameters

**Table 6.1:**  $A$  and  $B$  parameters for the cable class

Wire Class	Min Temp limit [°C]	Upper temp limit [°C]	Temp to withstand for 240 hours [°C]	Temp to withstand for 6 hours [°C]	A	B
Class 1	-40	85	110	135	$1.71 \cdot 10^{-24}$	23057.56
Class 2	-40	100	125	150	$1.87 \cdot 10^{-25}$	24841.50
Class 3	-40	125	150	175	$4.69 \cdot 10^{-27}$	27962.29
Class 4	-40	150	175	200	$1.17 \cdot 10^{-28}$	31267.53
Class 5	-40	175	200	225	$2.93 \cdot 10^{-30}$	34757.21
Class 9	-40	115	140	165	$2.05 \cdot 10^{-26}$	26691.84

The maximum operating range of the cable for the different classes is 180°C, according to Table 6.1. The  $A$  and  $B$  constants proportionally decrease from class 1 to class 5 with an increase in the maximum temperature limit of the cable class. Therefore, it can be concluded that with an increase in the maximum temperature limits, the temperature withstanding capacity or the current carrying capacity of the cable also increases. These empirical constants are used in (3.30) to calculate the life and thereby the damage value of the cable.

### 6.1.4 Impact of aggressiveness on damage value for basic drive cycles

Figure 6.3 shows the damage values of the basic drive cycles discussed in Section 4.5.1, for a class 5 cable.

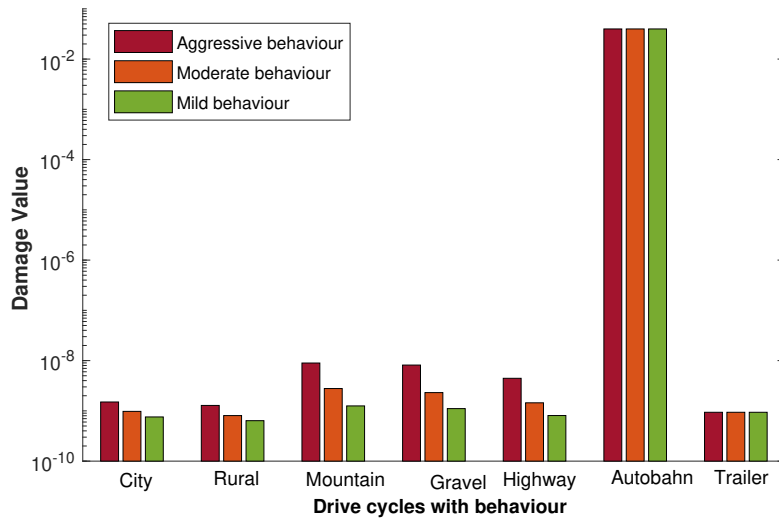


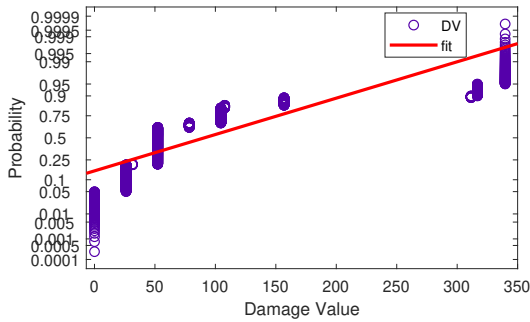
**Figure 6.3:** Comparison of the damage value for basic drive cycles based on behaviour and  $d_{tot} = 350000 \text{ km}$ .

The damage values shown in Figure 6.3 are computed for a total mileage of  $d_{tot} = 350000 \text{ km}$ , and it is observed that the distance-based cycles cause the least damage to the cables when compared to the event-based cycles. The event-based cycles reach higher temperatures within a short duration, as observed in Figure 6.2. The autobahn cycles contribute to a damage value nearing 1. This is explained by the peak temperature behaviour of the autobahn cycles shown in figure 6.2(a).

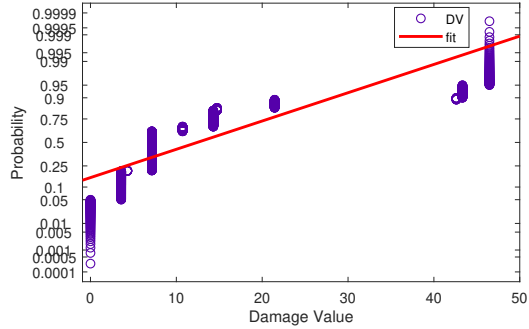
In the distance-based cycles, the mountain cycles have the highest damage value followed by the gravel and highway cycles; whereas the city and rural cycles contribute the least damage to the cables. It is observed that in each of these drive cycles, the aggressive cycles have the highest damage values, followed by the moderate and mild cycles. Therefore, the maximum speed cycle, namely the autobahn contributes to the maximum damage of the cable properties followed by the mountain cycle. The aggressive usage of the drive cycles over a long period of time damages the cable insulation faster than the other moderate and mild drive cycles, thus contributing to the cable reaching its end-of-life quicker.

### 6.1.5 Damage value spectra for customer population

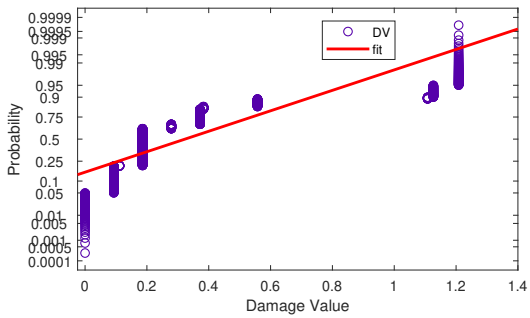
Figure 6.4 presents the probability plot of damage value, from the method described in Section 4.6 for the synthetic customer population, generated by the method discussed in Section 4.5, for the different cable classes.



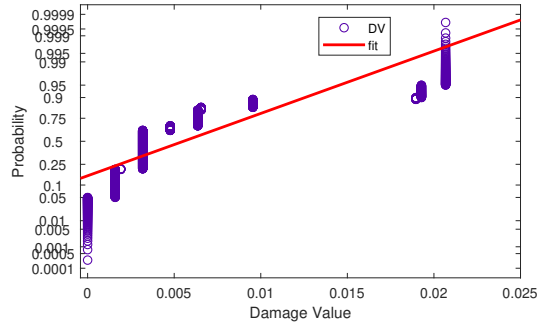
Cable class 1



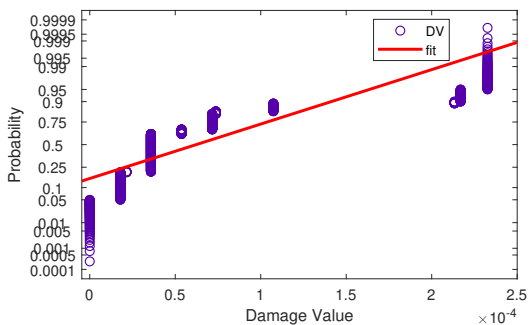
Cable class 2



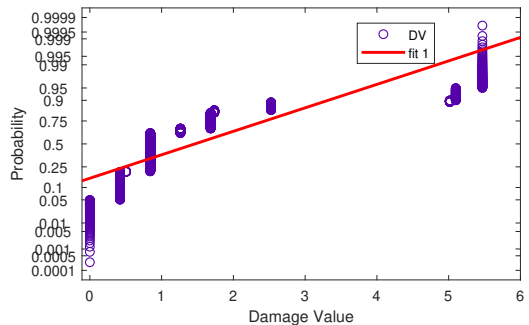
Cable class 3



Cable class 4



Cable class 5



Cable class 9

**Figure 6.4:** Damage value analysis for customer population for different classes at  $d_{tot} = 350000 \text{ km}$

It is observed that the customers using class 1 cables cause heavy damage, where the damage values are in the range of  $10^2$ . Similarly, the damage values

exceed a value close to one for cable classes 2, 3 and 9. When the damage value exceeds the limit of 1, it deteriorates the cable insulation, and thus the cable reaches its useful life. Whereas for class 4 and class 5 cables, the damage values are well within the limit of 1 and so these two classes can be considered for an improved cable design/selection.

### 6.1.5.1 Selection of cable class

Figure 6.5 presents the damage values for the 90<sup>th</sup> percentile customer, compared and analysed for different cable classes.

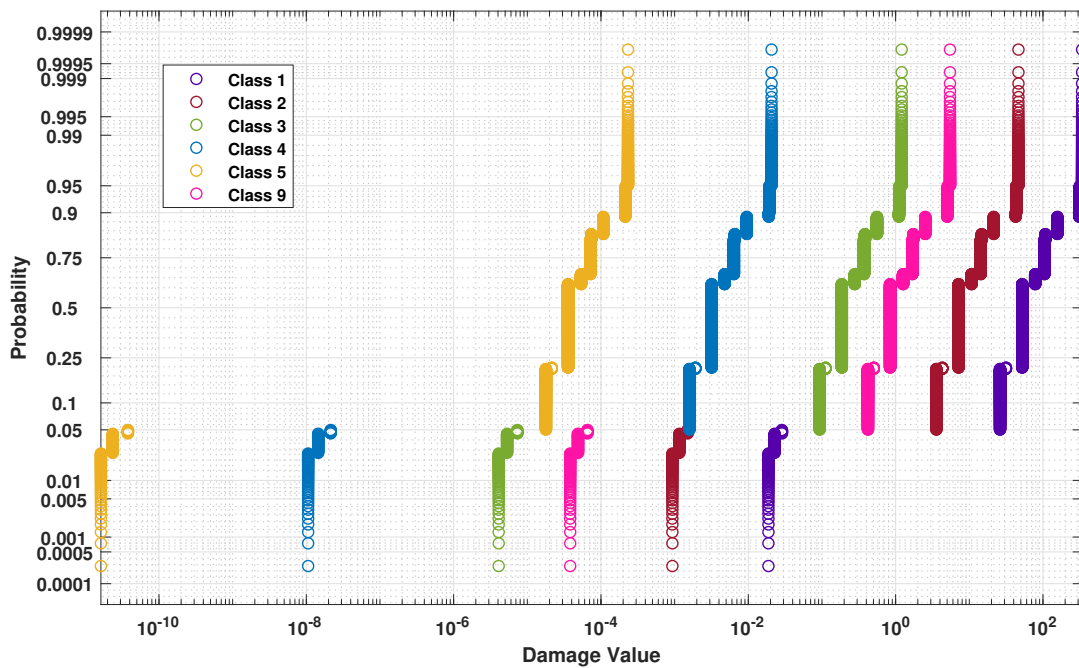


**Figure 6.5:** Comparison of damage value for different classes

From the probability plot discussed in the above section, it was concluded that both class 4 and class 5 could be considered for the selection of cables. Therefore, it is observed from Figure 6.5 that for a 90<sup>th</sup> percentile customer class 4 cable, the damage value is  $10^{-2}$  and is within the condition stated from Miner's rule, see Section 3.2.2. Thus, class 4 cables are the best-fit cable model which is further used to select the 90<sup>th</sup> percentile customer. Also an important observation is that the 90<sup>th</sup> percentile customer does not change with the cable class as their share in each drive cycle remains the same irrespective of the cable class.

### 6.1.5.2 Selection of 90<sup>th</sup> percentile customer

Figure 6.6 gives the cumulative distribution analysis, computed from the method discussed in 4.6, for the 90<sup>th</sup> percentile customer based on the best-fit cable model.

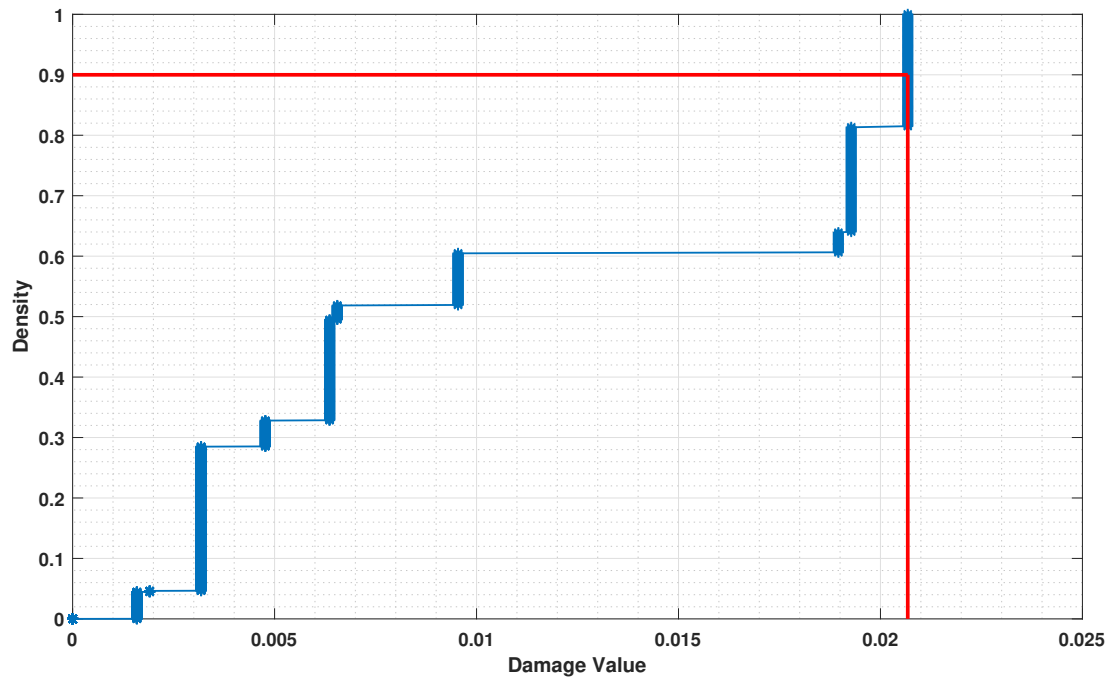
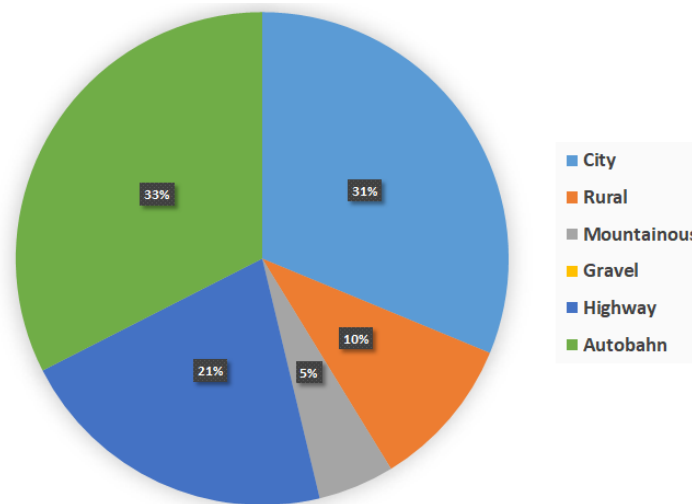


Figure 6.6: 90<sup>th</sup> percentile plot

The 90<sup>th</sup> percentile customer's name is re-traced based on their damage value from the customer population spectra. Thus, in this thesis, the 90<sup>th</sup> percentile customer was found to be 'Plain autobahn driver' as seen in Figure 4.12 with the damage value of  $2.06 \cdot 10^{-2}$ .

## 6.2 Creating current cycles for 90<sup>th</sup> percentile customer

Figure 6.7 shows the percentage share of the 90<sup>th</sup> percentile customer selected.



**Figure 6.7:** Drive cycle share for 'Plain autobahn driver'

The 90<sup>th</sup> percentile customer has a maximum share in the Autobahn cycle (33%) and with City cycle (31%). The distribution is used to create the current cycle based on the distance covered in each drive cycle and the driver behaviour. Figure 6.8 shows the distribution of the 90<sup>th</sup> percentile customer considering the aggressiveness of the driver in each drive cycle.

Environment distributions	Plain Autobahn driver [%]	Drive Cycle Behaviour	Drive Cycle Distance (length) [km]	Number of repetition of drive cycle
City	31.3	Aggressive	80.38	136
		Moderate	80.38	680
		Mild	80.38	544
Rural	10	Aggressive	94.28	37
		Moderate	94.28	185
		Mild	94.28	148
Mountain	5	Aggressive	127.45	13
		Moderate	127.45	68
		Mild	127.45	54
Gravel	0	Aggressive	193.66	0
		Moderate	193.66	0
		Mild	193.66	0
Highway	21.3	Aggressive	104.73	71
		Moderate	104.73	355
		Mild	104.73	284
Autobahn	32.5	Event -based	102.25	1112
Trailer	0	Event-based	8.2	0

**Figure 6.8:** Total share of the Plain autobahn driver with number of repetition in each drive cycle

The number of repetitions of each drive cycle is defined based on the the share shown in Figure 6.7, which is given as a pre-requisite to cable manufacturers to determine the current cycles of the 90<sup>th</sup> percentile customer. According to this study, it can be concluded that for the 90<sup>th</sup> percentile customer selected, the cable does not reach it's end-of-life for total distance of  $d_{tot} = 350000 \text{ km}$  which means that the cable is not completely damaged and has residual operating life.

### 6.3 Influence of ambient temperature on the cable usage

BEVs have market in different regions of the world, and based on an assumption, the influence of different ambient conditions of  $0^{\circ}\text{C}$ ,  $20^{\circ}\text{C}$ ,  $65^{\circ}\text{C}$  on the cable life is analysed for a class 4 cable and total mileage of  $350000\text{ km}$  as shown in Figure 6.9.

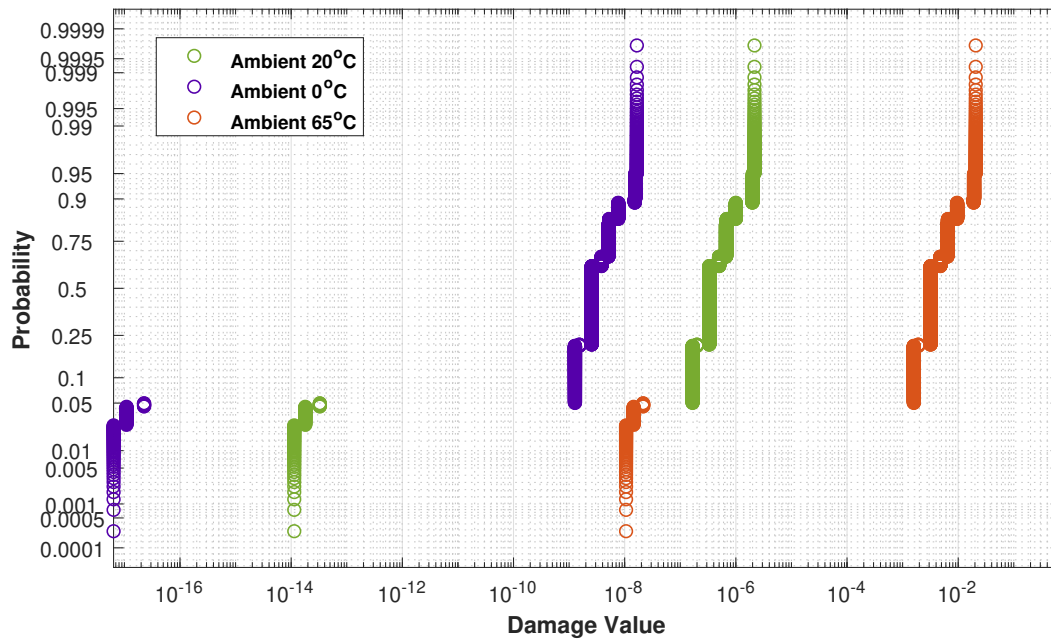


**Figure 6.9:** Comparison of damage value for different ambient temperature and  $350000\text{ km}$

The damage values for the  $90^{\text{th}}$  percentile customer based on usage is analysed. In very cold regions having an ambient temperature around  $0^{\circ}\text{C}$ , the  $90^{\text{th}}$  percentile customer shows a damage value of  $1.6 \cdot 10^{-8}$  whereas in hot regions having an ambient of up to  $65^{\circ}\text{C}$ , the damage value is reaches close to 1, nearing the lifetime of the cable. But in the case of moderate regions with an ambient temperature of  $20^{\circ}\text{C}$ , the damage value of the  $90^{\text{th}}$  percentile customer is  $2.16 \cdot 10^{-6}$ . Thus with increase in ambient conditions, the cables are utilised at higher rates.

## 6.4 Influence of convective cooling on the cable usage

Figure 6.9 shows the impact of natural and forced convective cooling on the cable life for a class 4 cable.

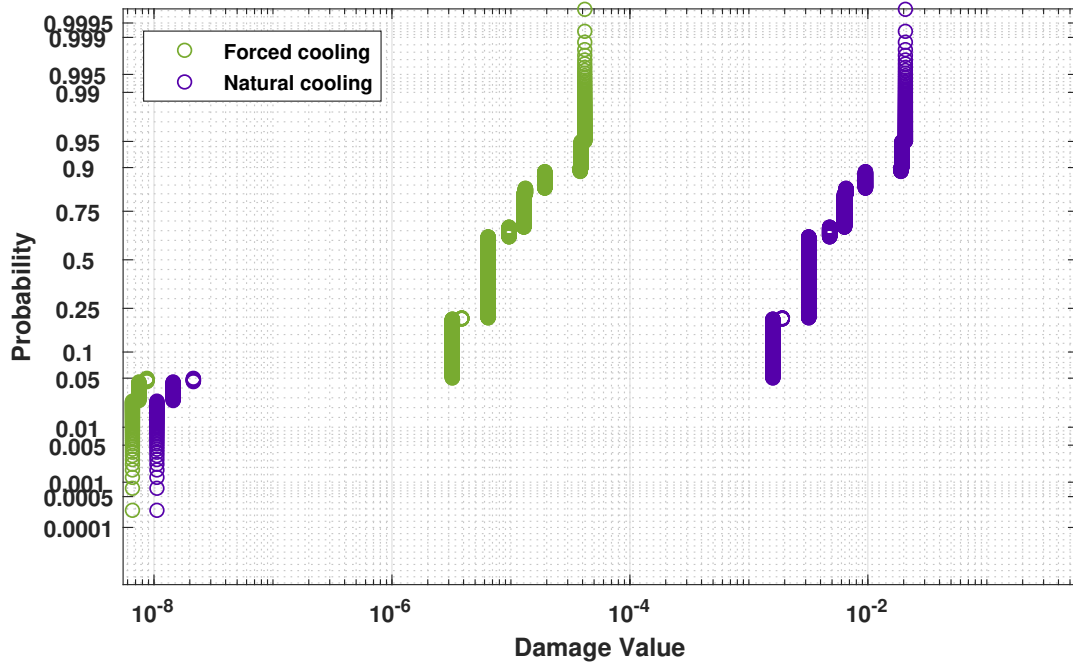


**Figure 6.10:** Comparison of damage value for with natural and forced convective cooling

With the effect of natural convective cooling (assumed as a closed chamber with negligible amount of convective heat transfer and validated temperature as in data-sheet A.1) is calculated from (3.14) in the thermal circuit of the cable, see Figure 3.3, the damage value reduces to  $5.2 \cdot 10^{-4}$  from  $9 \cdot 10^{-1}$  obtained forced convection cooling ( $h=40$ ) for the 90<sup>th</sup> percentile customer. Therefore, forced air cooling due to very high airflow reduces the time taken for the cable to reach its lifetime. Usually ( $h=40$ ) is a high value, ( $h=5$ ) or ( $h=10$ ) could be considered.

## 6.5 Impact of mileage accumulation and fast charging on cable ageing

The impact of mileage accumulation and fast charging on the life of the cable is investigated. A fast charging current cycle was created based on the realistic charging pattern of a charger. In this study, a CHAdeMO charger is considered for fast charging in BEVs delivering up to 50 kW charger, giving a maximum output voltage of 400 V DC and maximum output current of 125 A [21]. A fast charging current profile of battery for BEVs can be observed in Figure 6.11.

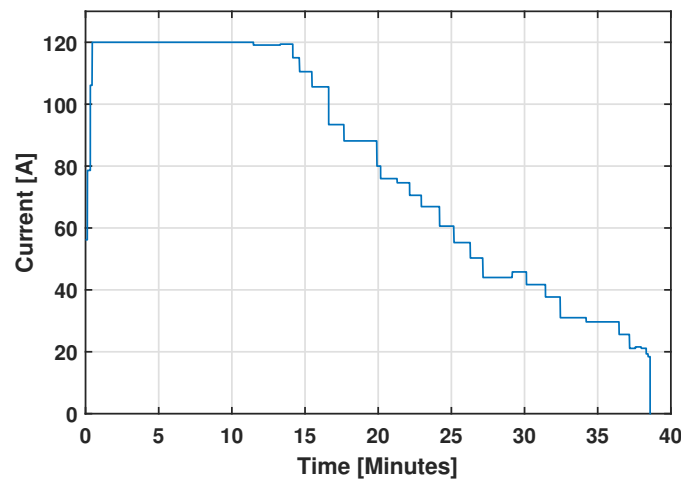


**Figure 6.11:** Realistic fast charging current profile according to [21]

The full charging takes about 40 *min* with the maximum SOC of 94%. The charging time varies based on the ambient temperature, during the winter, the charging time increases up to 90 *min*, and in extreme situations, it could take 4 *hours* [21]. It can be observed from Figure 6.11 that the current is constant until the 15<sup>th</sup> minute, and later it starts to reduce until the battery reaches full charge.

To consider the typical driving and charging occasions, a synthetic driving and charging pattern based is developed based on assumptions and study. A combination of different driving behaviours and driving cycles is developed where the people in the city do not only drive in the city cycle, but they drive and also charge in the nearby locations such as in the highway cycle, rural cycle, mountain cycle and multi cycles (long-distance trips). The basic drive cycles discussed in Section 4.5.1 are used to create different driving scenarios with charging profile and regular intervals to analyse the impact on the cable lifetime.

Figure 6.12 shows the selected combinations of drive cycles and fast charging profiles based on the assumed location of fast charging stations.

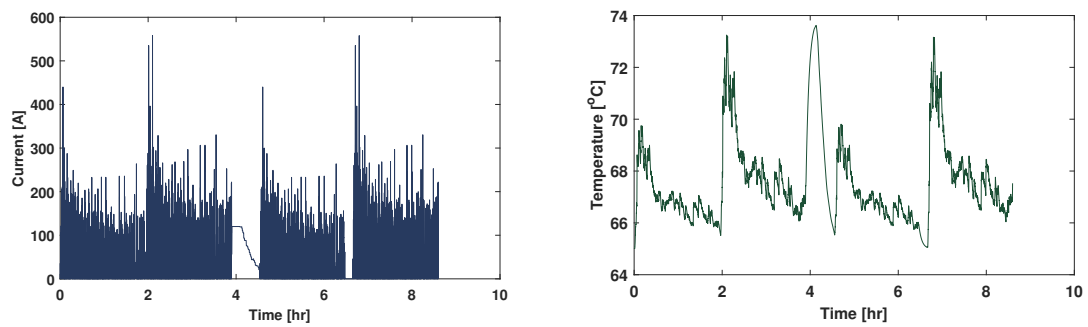
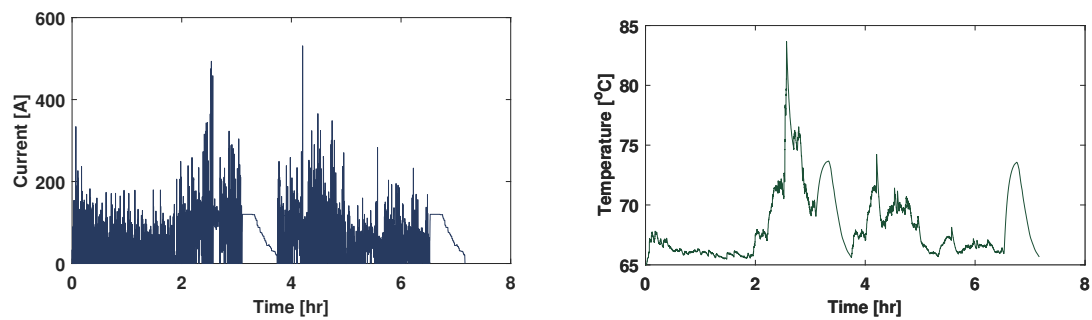
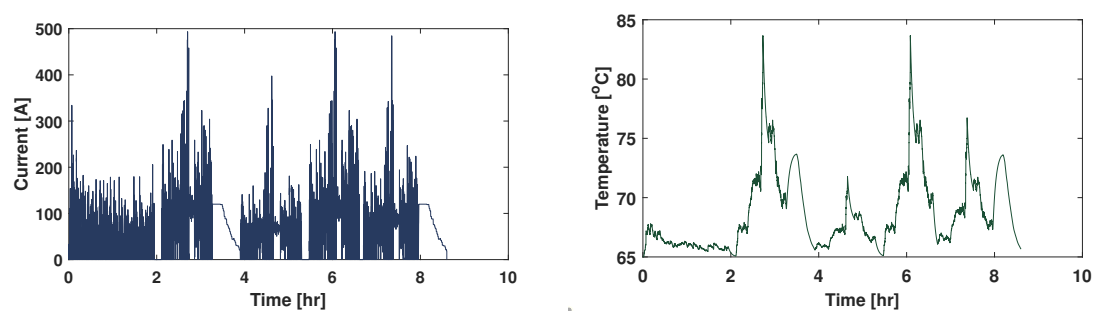
Type	Driving and Charging Pattern	Distance [Km]
City		321.52
Highway		604.13
Regional		373.67
Mountain		651.29
Multi Cycle 1		783.17
Multi Cycle 2		538.42

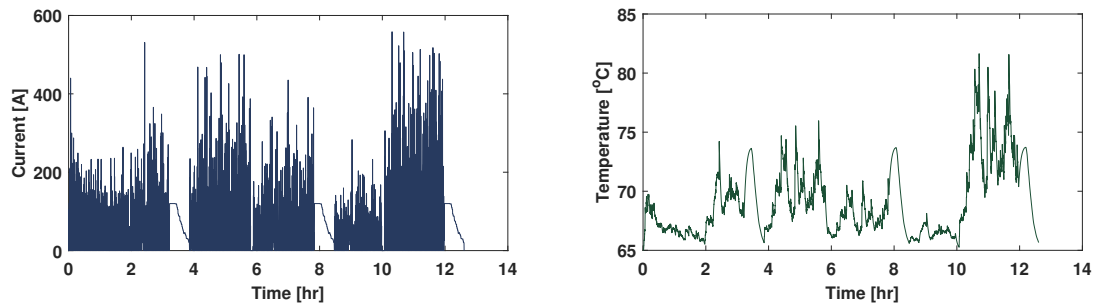
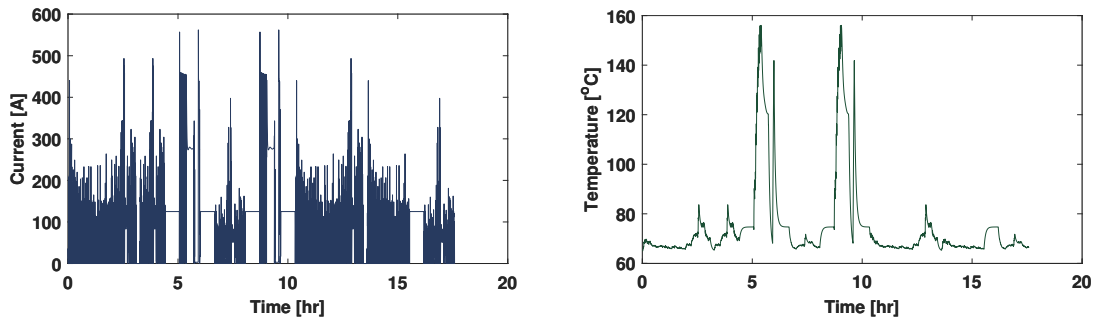
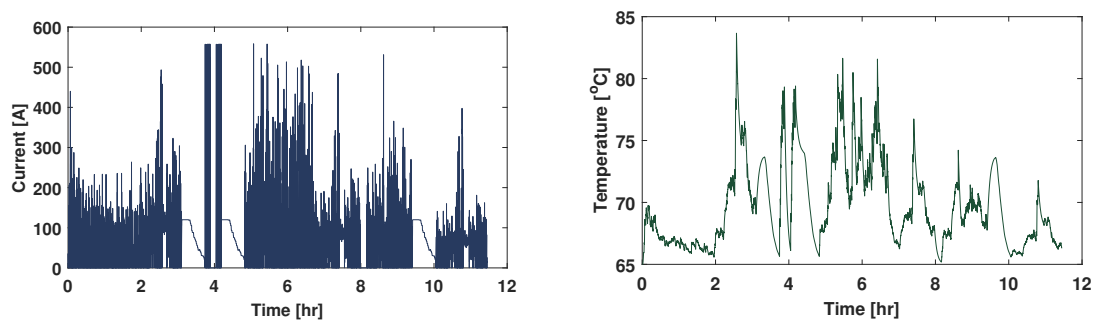
**Figure 6.12:** Driving pattern and charging cycles

The city and regional drive cycles are the most commonly used drive cycles to cover short distances, so one fast charging interval is used whereas the highway and mountain drive cycles covers about 600 km and have 2-3 fast charging intervals. But the multi cycles represent long-distance trips with three or more fast charging intervals. The impact of these combined cycles with fast charging on the conductor temperature is discussed in detail in the next section.

### 6.5.1 Impact of combined drive cycles on cable conductor temperature

The driving pattern influences the ageing of the characteristic cable properties due to the loading, as discussed in the previous chapters so far. This analysis is further extended to understand the usage of cables when used for charging purposes. The charging requirements of electric vehicles are determined to a great extent by the factors: charging location, charging need, and the charging moment [26]. Based on these factors, necessary assumptions were made to create a combination of driving cycles for different duration trips, as shown in Figure 6.12. Thus the impact of combined drive cycles and fast charging on the life of the cable is analysed in detail in this section.

**Case 1: City cycle****Figure 6.13:** Simulated City current cycle and cable temperatures**Case 2: Regional cycle****Figure 6.14:** Simulated Regional current cycle and cable temperatures**Case 3: Highway cycle****Figure 6.15:** Simulated Highway current cycle and cable temperatures

**Case 4: Mountain cycle****Figure 6.16:** Simulated Mountain current cycle and cable temperatures**Case 5: Multi Cycle 1****Figure 6.17:** Simulated Multi-Cycle 1 current cycle and cable temperatures**Case 6: Multi Cycle 2****Figure 6.18:** Simulated Multi-Cycle 2 current cycle and cable temperatures

For the fast charging analysis, the cables temperatures for the different driving scenarios are calculated based on the temperature calculation method discussed in Section 4.3. The current cycles and temperature plots are simulated for the different use-cases defined, seen in Figure 6.12. Figure 6.17 has the highest number of charging intervals and the cycle duration is almost 17.8 *hours*. The Multi-Cycle 1 is observed to reach very higher peak temperatures, almost 160°C than the other

cycles. It is observed from Figure 6.18 that the current reaches the same peak of  $560 A$  as that of Multi-Cycle 1, but the temperature peak reaches only close to  $85^{\circ}C$  for lesser charging intervals.

### 6.5.2 Damage value analysis for combined drive cycles

Figure 6.19 and table 6.2 presents the calculated damage values for the combined drive cycles as shown in Figure 6.12 for a total mileage of  $d_{tot} = 350000 km$ . Also presents the influence of with and without fast charging in the combined drive cycles shown in Figure 6.12.

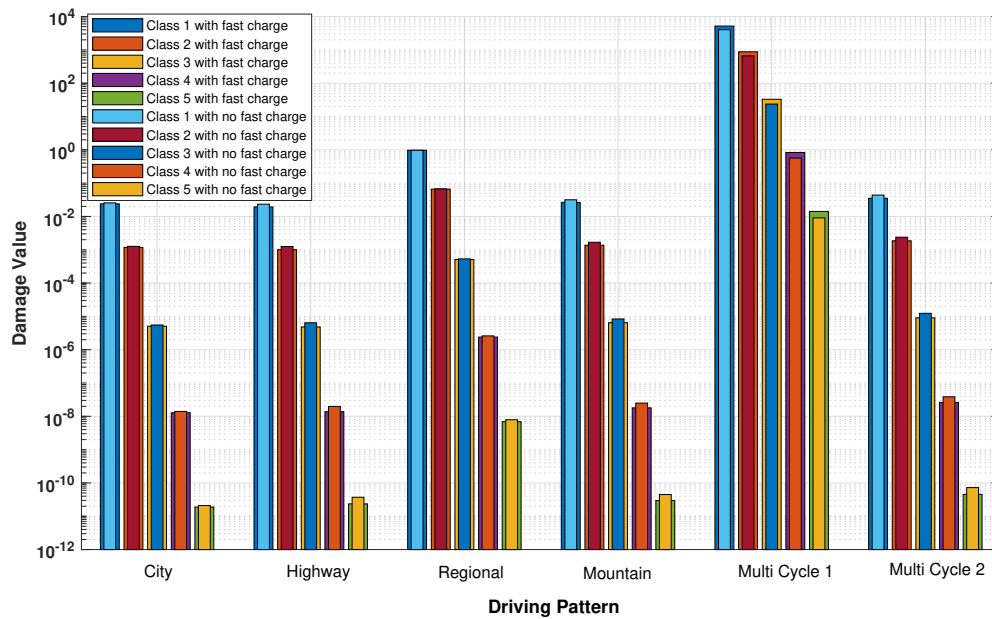


**Figure 6.19:** Analysing the usage of the cable for different classes during combined drive cycles, combined drive cycles with fast-charging represents much solid bar graph and combined drive cycles without fast-charging represents finer bar graph, and a total distance cover of  $d_{tot} = 350000 km$

**Table 6.2:** Damage value of cable for different cable classes during during combined drive cycles with fast charging and  $d_{tot} = 350000 km$

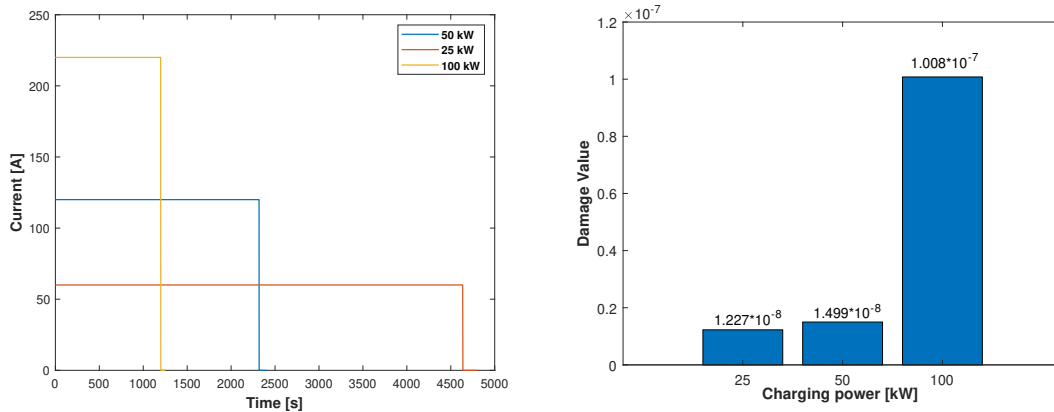
Environment	Cable Class 1	Cable Class 2	Cable Class 3	Cable Class 4	Cable Class 5
City	$2.388 \cdot 10^{-2}$	$1.176 \cdot 10^{-3}$	$5.073 \cdot 10^{-6}$	$1.279 \cdot 10^{-8}$	$1.889 \cdot 10^{-11}$
Highway	$1.930 \cdot 10^{-2}$	$1.004 \cdot 10^{-3}$	$4.808 \cdot 10^{-6}$	$1.374 \cdot 10^{-8}$	$2.353 \cdot 10^{-11}$
Regional	$2.267 \cdot 10^{-2}$	$1.162 \cdot 10^{-3}$	$5.409 \cdot 10^{-6}$	$1.498 \cdot 10^{-8}$	$2.481 \cdot 10^{-11}$
Mountain	$2.651 \cdot 10^{-2}$	$1.369 \cdot 10^{-3}$	$6.440 \cdot 10^{-6}$	$1.795 \cdot 10^{-8}$	$2.975 \cdot 10^{-11}$
Multi Cycle 1	$5.19 \cdot 10^3$	876.5	32.9	0.83	$1.4 \cdot 10^{-2}$
Multi Cycle 2	$3.5215 \cdot 10^{-2}$	$1.854 \cdot 10^{-3}$	$9.046 \cdot 10^{-6}$	$2.625 \cdot 10^{-8}$	$4.541 \cdot 10^{-11}$

Figure 6.19 compares the damage value of driving scenarios for different classes of cables and also compares the influence of with and without fast charging

on the cable life. The damage values are calculated according to Table 6.2. It is observed that for the total mileage, the Multi-Cycle 1 results in the highest damage value to the cables in all the cable classes used, due to continuous usage of the drive cycles. It is also observed that for class 4 and class 5 cables the damage values are within the limit of 1, and the addition of 50 kW fast charger doesn't influence much on the cable life since the temperature values are under cable operating temperature range.

### 6.5.3 Influence of different charging rates on cable life

Figure 6.20 and Figure 6.21 presents the charging rates of 25 kW, 50 kW and 100 kW available in different fast-charging stations.



**Figure 6.20:** Fast charging current profile at different charging stations **Figure 6.21:** Damage value due to different charging rates and drive cycles

The calculated conductor temperature of the City cycle with combined drive cycles and fast charging according to Figure 6.13 for a class 4 cable is used in this study. With an increase in power ratings, the charging duration reduces due to the increase in charging speed, as observed in Figure 6.20. For the same combined cycle, the damage value to the cable increases with higher fast charging current profile as observed in Figure 6.21. Further, the effect of damage to the cable due to 25 kW and 50 kW charging do not differ much. The 100 kW charging on the other hand, has a large impact.

# 7

## Conclusion

The presented method determines which usage pattern to consider when choosing a HV cable in BEVs. Initially, the LPN model of the HV cable was developed, and the temperature profiles of the cables were studied. The parameters of the temperature model were compared to the supplier data-sheet, and it was found that they were close enough for all the temperature ranges. The Arrhenius ageing model of a cable was implemented to evaluate the useful life of the cable. The Arrhenius constants  $A$  and  $B$  were determined for different classes of cables, and then the accumulated damage value of the cable was computed over the entire life of the cable.

This work aims to provide a more extensive analysis of the usage and model the damage mechanism for BEVs. First, different driver types were created, and the distribution of driver types in different drive cycles was defined. Then the frequency split was given to the drivers depending upon their occurrence. From the driver types and driver behaviour, a synthetic customer population was generated. Further from the results of this study, a statistical analysis was done, and the 90<sup>th</sup> percentile was selected. Since this work has aimed to provide a realistic usage pattern, the usage of the current cycle for the 90<sup>th</sup> percentile was determined based on the number of repetitions in each drive cycle. Furthermore, the influence of the convective heat transfer and the ambient temperature on the cable life was studied.

Finally, an additional investigation was done to determine the influence of fast charging on the life of the cables. A realistic current cycle was developed with different scenarios which include fast charging current cycles and the current cycles obtained by the usage in different drive cycles.

### 7.1 Future work

- The scope can be further extended by analysing the usage of other HV components (fuse, contactor, and connector). It is essential to understand the complete utilisation of the HV system since the selection criteria of these components are interdependent. For example, by using the ageing model of the fuse, contactors and connectors with that of HV cables, would present a clear view to analyse usage of the entire HV system. During the study of a fuse, the number of repeated current cycles has to be considered to understand the time to melt the fuse ( $I^2t$ ).
- And one cannot be particular that the ageing of components holds adequate for

real-time ambient conditions. So the damage calculations of components can signify a high degree of accuracy by considering the real ambient conditions around the HV system.

- In general, uncertainty in simulation inputs on the influence on electrical energy transfer due to different drive cycles could be studied with more accuracy by using real data of the customers. In this work, the drive cycles generated from the vehicle simulations were only considered. But a pre-defined requirement of the different drive cycles could be given to analyse the influence of extreme current cycles.
- Furthermore, it would be interesting to deepen the study by doing the accelerated ageing tests on the components. So, one could measure the real parameters and compare them with the simulations.
- In this work, the damage values of the different customers are very close, since run-time of the vehicle simulation is only for 7000 s due to run-time errors. Therefore, to simulate complete drive cycles, the run-time should be extended to 10000 s, to observe more variations in customer behaviour.
- Another important aspect could be consideration of heat flow along the length-wise direction.

# Bibliography

- [1] Muhammad Buhari, Student Member, IEEE, Victor Levi, Senior Member, IEEE, and Selma K. E. Awadallah, Student Member, IEEE, "Modelling of Ageing Distribution Cable for Replacement Planning," *IEEE Transactions on Power Systems*, vol. 31, NO. 5, September 2016
- [2] Peter H.G.Allen, Arnold Tustin, "The Aging Process in Electrical Insulation:A Tutorial Summary," *IEEE Transactions on Electrical Insulation*, vol. EI-7, NO. 3, SEPTEMBER 1972
- [3] Endicott. H ,Hatch. B and Sohmer. R, "Application of the Eyring model to capacitor aging data," *IEEE Transactions on Component Parts*, vol. 12, 1965
- [4] Herrmann, Florian and Rothfuss, Florian, "Introduction to hybrid electric vehicles, battery electric vehicles, and off-road electric vehicles," *Advances in Battery Technologies for Electric Vehicles*,Elsevier, pp. 3–16, 2015
- [5] Electrical, ZVEI-German and Electronic Manufacturers Association and others, "Voltage Classes for Electric Mobility," Frankfurt am Main, Germany, 2013
- [6] Guzzella, Lino and Sciarretta, Antonio and others, "Vehicle propulsion systems," Springer, vol. 1, 2007
- [7] Michael Nicholas and Dale Hall,"LESSONS LEARNED ON EARLY ELECTRIC VEHICLE FAST-CHARGING DEPLOYMENTS," International Council on Clean Transportation, 2018
- [8] Jagannathan, Rajagopalan and Atzeri, Marco and Hoenes, Hans-Peter, "Power MOSFETs for Low Voltage and High Current Automotive Applications-48V Bus Systems," PCIM Europe 2017; International Exhibition and Conference for Power Electronics, Intelligent Motion, Renewable Energy and Energy Management, VDE, pp. 1–7, 2017
- [9] Electrical, ZVEI-German and Electronic Manufacturers Association and others, "48-Volt Electrical Systems – A Key Technology Paving to the Road to Electric Mobility," Frankfurt am Main, Germany, 2013
- [10] Schudeleit, Mark and Sieg, Christian and Küçükey, F, "The potential of 48V HEV in real driving," 16. Internationales Stuttgarter Symposium, Springer, pp. 837–854, 2016
- [11] MATTEWOS BERHANE TEFFERI, Coupled Electro-Thermal Model for Submarine HVDC Power Cables [Online], Available :

- <http://publications.lib.chalmers.se/records/fulltext/179477/179477.pdf>
- [12] Reichert and Heinz, "High Voltage Power Connector for Automotive Hybrid and Electric Drive Components," *The Automotive TM, HEV EV Drives magazine* by CTI, 05 2014
- [13] Hughes, Timothy James, "Environmental controls on the state of HV cables under the seafloor," University of Southampton, 2016
- [14] Sonja Tidblad, Lundmark Mikael, Alatalo Torbjörn Thiringer and Emma Arfa Grunditz, *VEHICLE COMPONENTS AND CONFIGURATIONS* [Online], Available : [http://publications.lib.chalmers.se/records/fulltext/211435/local\\_211435.pdf](http://publications.lib.chalmers.se/records/fulltext/211435/local_211435.pdf)
- [15] T. Robbins, "Fuse Model for Over Current Protection Simulation of DC distribution systems," Telecom Australia Research Laboratories
- [16] Erik Figenbaum, "Charging into the future Analysis of fast charger usage," Institute of Transport Economics, ISSN 2535-5104 *Electronic*, Oslo, January, 2019
- [17] Xin, Q, "Durability and reliability in diesel engine system design," *Diesel Engine System Design*, pp. 113–202, 2013
- [18] Jerome Jacob Mies, Jurjen Rienk Helmus and Robert van den Hoed, "Estimating the Charging Profile of Individual Charge Sessions of Electric Vehicles in The Netherlands," *World Electric Vehicle Journal*, 22 June 2018
- [19] Muhammad Buhari, "Reliability Assessment of Ageing Distribution Cable for Replacement in Smart Distribution Systems," University of Manchester, 2016
- [20] Brancato, EL, "Insulation aging a historical and critical review," *IEEE Transactions on electrical Insulation*, no. 4, IEEE, pp. 308–317, 1978
- [21] Aaron Loiselle-Lapointe, Ian Whittal, and Martha Christenson, "Electric Vehicles: Impacts of Mileage Accumulation and Fast Charging," *World Electric Vehicle Journal* Vol. 8, ISSN 2032-6653, WEVA, 2016
- [22] Lei, Ming and Liu, Gang and Lai, Yu-ting and Li, Jin-zhu and Li, Wenxiang and Liu, Yi-gang, "Study on thermal model of dynamic temperature calculation of single-core cable based on Laplace calculation method," 2010 IEEE International Symposium on Electrical Insulation, pp. 1–7, 2010
- [23] Ilgevičius, A and Liess, H-D, "Calculation of the heat transfer in cylindrical wires and electrical fuses by implicit finite volume method," *Mathematical Modelling and Analysis*, Vol. 8, no. 3, Taylor & Francis, pp. 217–227, 2003
- [24] Scarpa, Federico and De Rosa, Mattia, "Transient heat conduction in wires with heat sources; lumped and distributed solution techniques," *Heat Transfer Research*, Vol. 47, no. 8, Begel House Inc., 2016
- [25] Yang, Lin and Qiu, Weihao and Huang, Jichao and Hao, Yanpeng and Fu, Mingli and Hou, Shuai and Li, Licheng, "Comparison of conductor-temperature calculations based on different radial-position-temperature detections for high-voltage power cable," *Energies*, Vo. 11, no. 1, pp. 117, Multidisciplinary Digital Publishing Institute, 2018

- [26] Hijazi, Alaa and Kreczanik, Paul and Bideaux, Eric and Venet, Pascal and Clerc, Guy and Di Loreto, Michael, "Thermal network model of supercapacitors stack," , IEEE Transactions on Industrial Electronics, Vol. 59, no. 2, pp. 979–987, IEEE, 2011
- [27] Grahn, Pia, "Electric vehicle charging impact on load profile," KTH Royal Institute of Technology, 2013
- [28] Arora, Jasbir S, "Chapter 20: Additional Topics on Optimum Design," Introduction to Optimum Design, McGraw Hill International Edition, Vol. 3, pp. 731–784, 1989
- [29] PIPKORN, LINDA, "XC90 Plug-in Hybrid Customer Usage', Chalmers University of Technology, 2018
- [30] Grunditz, Emma, "Bev powertrain component sizing with respect to performance, energy consumption and driving patterns," Chalmers University of Technology, 2014
- [31] IEC, Calculation of the current rating –Part 2-1: Thermal resistance – Calculation of thermal resistance, IEC 60287-2-1:2015
- [32] ISO, Electrically propelled vehicles - Safety specifications-Part 3: Protection of person against electric shock, ISO 6469-3,December 2011
- [33] IEC, Electric cables - Calculation of the current rating - Part 1-1:Current rating equations (100 % load factor) and calculation of losses , IEC 60287-1-1:2014
- [34] SS-ISO 6722-1. Road vehicles-60V and 600V single-core cables-part 1: dimensions, test methods and requirements for copper conductor cables.





# A

## Appendix 1

### A.1 Cable conductor temperature plot from the data sheet

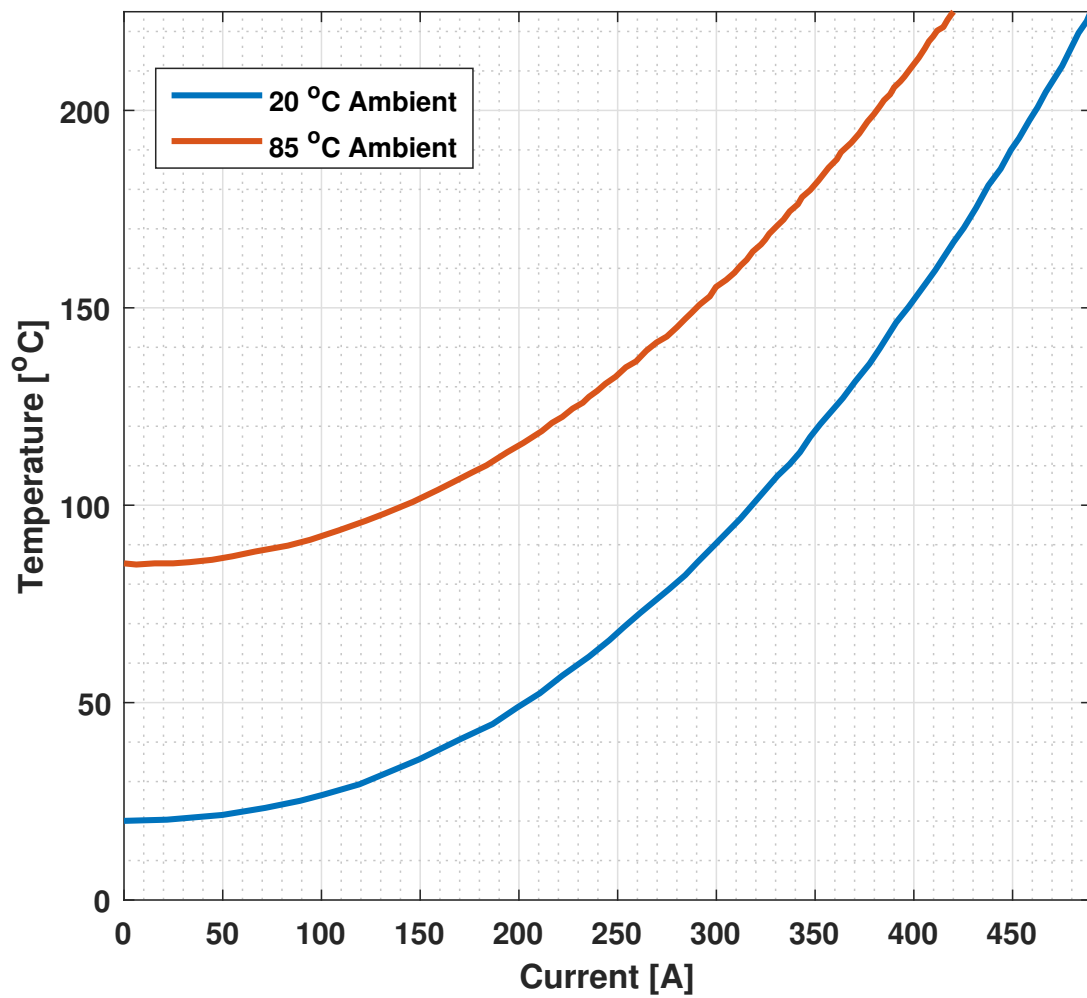


Figure A.1: Continuous current loading on conductor as a function of ambient temperature

## A.2 Cable parameters

### A.2.1 Geometrical parameters

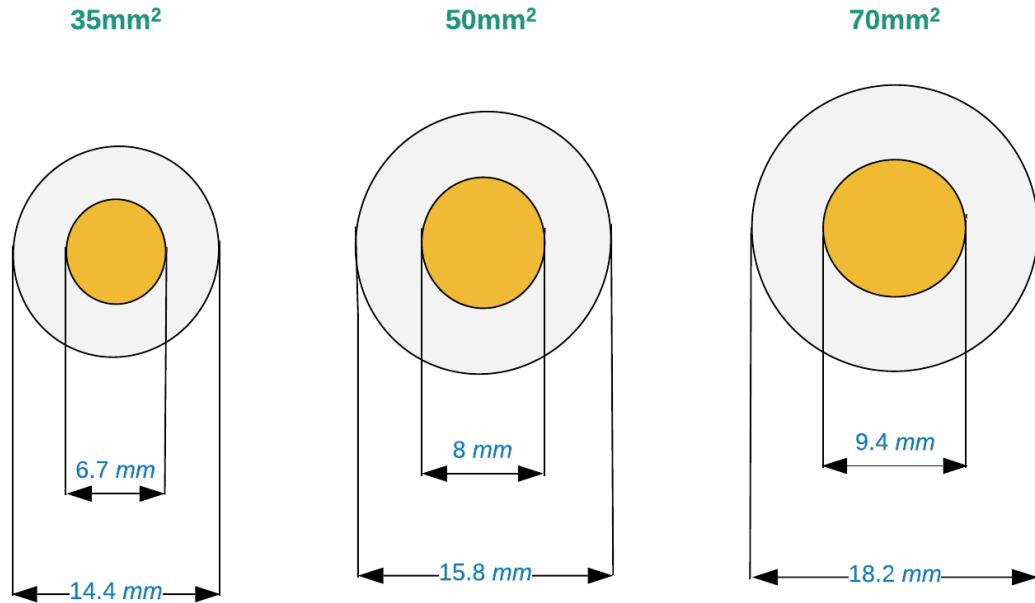


Figure A.2: Cable core conductor diameter and the insulation diameter

### A.2.2 Calculation of conductor temperature for steady state condition (50mm<sup>2</sup>)

Table A.1: Input parameters for the thermal calculations for the steady state condition

Input Parameters	Value
Specific Heat Capacity of copper $C_p$ [ $J/kgK$ ]	0.39
Temperature Coefficient of Resistance [ $\alpha$ ]	4
$R_{20}$ Conductor Resistance at 20°C (50mm <sup>2</sup> ) [ $m\Omega/m$ ]	0.368
Density of copper $\sigma_{Cu}$ [ $kg/m^3$ ]	8960
Thermal conductivity $k$	$(5.802 \cdot 10^{-4}) \cdot Tc + (-0.0246)$
Length of cable [ $m$ ]	1
Radius of conductor [ $mm$ ]	$4 \cdot 10^{-3}$
Radius of outer surface [ $mm$ ]	7.82
Current [ $A$ ]	100,200,300,400
Run time [ $sec$ ]	3600
Ambient Temperature [ $^{\circ}C$ ]	85

- Create a function  $dydt = bev(t, Tc, Tcycle, curr, IC)$  where  $t$  is time of the ODE solver,  $Tc$  is the conductor temperature,  $Tcycle$  is the total run time of the cycle,  $curr$  is the input current,  $IC$  is the initial condition,  $dydt$  is the the Ordinary differential equation. And define input parameters and the calculations for the differential equation.
- Using the ODE solver *ode23s*, define the output parameters of the ODE and call the defined function *cable* with the input parameters, input the time span, initial condition  $IC$ .

## A.2.3 MATLAB code for calculation of cable conductor temperature

### A.2.3.1 Input parameters code and save file name as:cable

---

```

1 function dydt = cable(t,Tc,Tcycle,curr,IC)
2
3 I_cable = interp1(Tcycle,curr,t); % Interpolate the data set
   (Tcycle,curr) at time t
4
5 %% Input parameters for the cable
6
7 alpha = 4e-3; % Resistance thermal coeff
8 R20 = 368e-6; % [OHMS/m] Constant at 20C 50mm2
9 %R20 = 527e-6; % [OHMS/m] Constant at 20C 35mm2
10 %R20 = 259e-6; % [OHMS/m] Constant at 20C 70mm2
11 Cp = 0.39*1e3; % [J/Kg*K]
12
13 %% Geometry input
14
15 Area_cs=50*1e-6; % [m] for 50mm2
16 outer_dia=15.8*1e-3; %[m] for 50mm2
17
18 %Area_cs=70*1e-6; % [m] for 70mm2
19 %outer_dia=18.2*1e-3; %[m] for 70mm2
20
21 % Area_cs=35*1e-6; % [m] for 35mm2
22 % outer_dia=14.4*1e-3; %[m] for 35mm2
23
24 length_of_cable=1;% length of cable [m]
25
26 %% Thermal conductivity of cable insulation for diff cable
27
28 poly85 = [5.802654029868824e-04 -0.024625676540822]; %50mm2
29 k=poly85(1)*(Tc)+(poly85(2)); %50mm2
30
31 % poly85 = [6.005720510797214e-04 -0.025332577374489]; %35mm2
32 % k=poly85(1)*Tc+(poly85(2)); %35mm2

```

---

```

33
34 %poly85 = [5.849338686875862e-04 -0.015984689097001]; %70mm2
35 %k=poly85(1)*Tc+(poly85(2)); %70mm2
36
37 Radius_copperwire=(sqrt(Area_cs/pi));%radius of the copper wire[m]
38 Insulation_thickness=(outer_dia-(2*Radius_copperwire));%insulation
    thickness [m]
39 Area_conductance = 2*pi*Radius_copperwire*length_of_cable;
40 Radius_insulation=(outer_dia/2);
41 density_copper= 8960;% density of copper wire [Kg/m^3]
42 Volume_wire = pi*Radius_copperwire^2*length_of_cable; % [m^3]
43 mass = Volume_wire*density_copper;% [kg]
44
45 Rth = (k*(Area_conductance /Insulation_thickness)); % Thermal resistance(
    equals 1/Rth)
46 R_cable= ((R20)*(1+(alpha.*(Tc-293.15))));
47 P= (I_cable.^2.*R_cable); % Power Input (I^2*R)
48 P_loss=((Tc-IC).*Rth);% Power loss in insulation and to Ambient
49 T_1= (1/(Cp*mass)*(P-P_loss));
50 dydt=T_1;

```

---

### A.2.3.2 Execution code or Run code and and save file name as:cable1

---

```

1 clear all
2 clc
3 %%
4 % Write a function to interpolate the data sets specified above to obtain
    the value of the time-dependent terms at the specified time:
5 t_start=0;
6 t_end= 60*60; % Run time of 3600 sec
7 Tcycle=linspace (0 ,t_end, 10);
8 for n=1:4
9 i=[100 200 300 400]; % Input current
10 curr=abs(i(n)+1e-9*Tcycle); % Vector correction
11 %
12 %%
13 Tamb=85; %Ambient Temperature
14 tspan = [t_start t_end];
15 IC = Tamb+273.15; % to Kelvin
16 opts = odeset('RelTol',1e-6,'AbsTol',1e-9); % Tolerance
17 [time,Temp_Cu] = ode23s(@(t,Tc)
    cable(t,Tc,Tcycle,curr,IC),tspan,IC,opts); % Solve ODE using
    ode23s
18 %
19 %% Plot
20 figure(1)
21 plot(time, Temp_Cu-273.15, '-b');
22 xlabel('Time [sec]');

```

## A. Appendix 1

---

```
23 ylabel('Tc [°C]');  
24 hold on  
25  
26 n=n+1;  
27 end
```

---